Max-Planck-Institut
für Meteorologie

REPORT No. 237

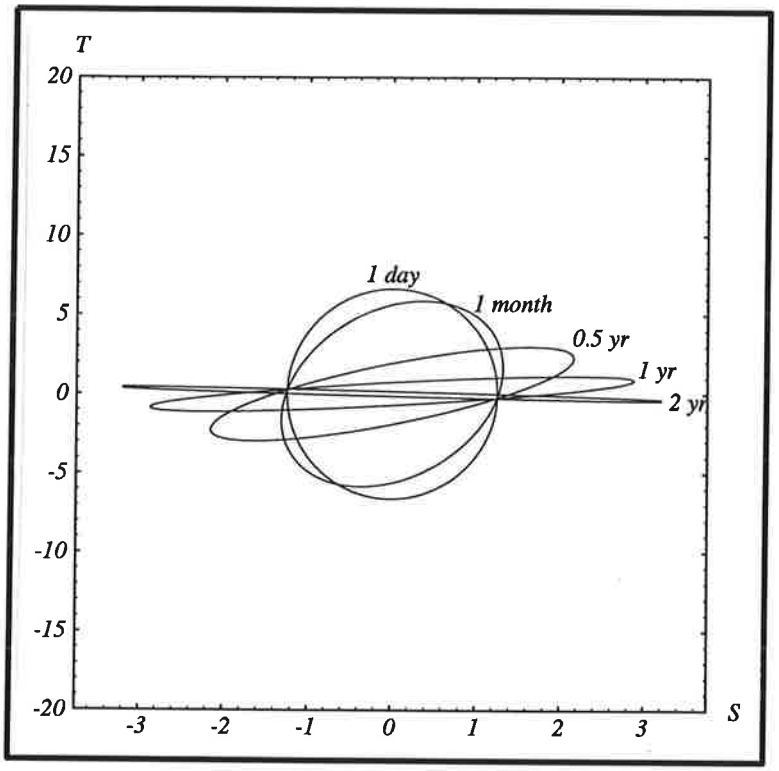

PART I: WHY ARE SALINITY ANOMALIES OF GREAT IMPORTANCE FOR LONG-TIME CLIMATE VARIABILITY? ANALYSIS OF SIMPLE CLIMATE MODELS

PART II: EXACT SOLUTION OF JACOBI TYPE EVOLUTION EQUATIONS

by

Gerrit Lohmann · Joachim Schneider

HAMBURG, May 1997

AUTHORS:

Gerrit Lohmann — Max-Planck-Institut für Meteorologie

Joachim Schneider — Fachbereich Physik
Philipps-Universität Marburg
Renthof 7
35032 Marburg/Lahn
Germany

MAX-PLANCK-INSTITUT
FÜR METEOROLOGIE
BUNDESSTRASSE 55
D - 20146 HAMBURG
GERMANY

Tel.: +49-(0)40-4 11 73-0
Telefax: +49-(0)40-4 11 73-298
E-Mail: <name> @ dkrz.de

ISSN 0937-1060

Why are salinity anomalies of great importance for long-term climate variability ? Analysis of simple climate models

Gerrit Lohmann[1]
Max-Planck-Institute for Meteorology, Hamburg, Germany

and Joachim Schneider[2]
University of Marburg, Marburg/Lahn, Germany

Journal: Journal of Physical Oceanography
April 1997

1: corresponding author:
Max-Planck-Institute for Meteorology
Bundesstrasse 55 Tel.: (0049) 40-41173 103
20146 Hamburg Fax: (0049) 40-41173 298
Germany email: gerrit.lohmann@dkrz.de

2: current affiliation: Data General Walldorf, Germany

ISSN 0937-1060

Abstract

We analyze the sensitivity of the ocean's thermohaline circulation using idealized models of the North Atlantic. The nonlinear Stommel (1961) box model is solved exactly. Using the analytical solution of a coupled atmosphere-ocean version of Stommel's model, we derive the critical salinity perturbation, necessary to induce a break down of the thermohaline circulation . We find that the glacial oceanic circulation with a weaker meridional overturning is more sensitive than the present one. The model reveals furthermore that the optimal perturbation affecting long-term climate variability is by high latitude haline forcing, although this perturbation has little resemblence with the most unstable mode of the system and the leading EOF.

The linear stage of the forecast error growth is analyzed in the box model. The amplification of the forecast error ellipsoide is largest for high latitude haline forcing, associated with maximum energy growth on times less than a decade. Sensitivity experiments with a more sophisticated coupled model reveal the basic mechanisms involved in the thermohaline circulation's response to sea surface salinity perturbations. The results qualitatively agree with those of the analytical model, although different mechanisms are responsible for the sensitivity. Our results are useful for the interpretation of paleoclimatic records and interdecadal climate variability.

1 Introduction

In the northern North Atlantic, warm and saline surface water is transported northward and is cooled and freshened through surface fluxes. The large amount of heat transported by the oceanic thermohaline circulation (THC) is responsible for the relatively mild climate in northern Europe. Most of the ocean's northward heat transport is associated with the meridional overturning which is driven, at least partly, by deep water formation in the Labrador and Nordic Seas.

In his pioneering work, Stommel (1961) has shown, using an ocean box model, that the THC can have multiple equilibria under the same atmospheric forcing. Stommel's result has been confirmed with a three dimensional ocean circulation model by Bryan (1986). Recently, numerical studies (Rahmstorf and Willebrand, 1995; Manabe and Stouffer, 1995) and theoretical studies (Marotzke and Stone, 1995; Lohmann et al., 1996 b) have shown that the sensitivity of the ocean models is largely overestimated when using fixed atmospheric temperature and fresh water flux because of atmospheric feedbacks.

There is, however, mounting paleoclimatic evidence (Boyle and Keigwin, 1987; Fairbanks, 1989; Keigwin et al., 1991) that secular variability and abrupt climate changes are linked to variations in the THC. Broecker et al. (1985) speculated that massive discharges of meltwater into the northern North Atlantic caused the Younger Dryas event where vegetation returned to a cold climate state over Europe. Paleo-temperature records (Dansgaard et al., 1993) show that after deglaciation the temperatures over North America and western Europe have dropped. Similar abrupt climate changes due to large freshenings were found analyzing sediment cores (Bond et al., 1992; Sarnthein et al., 1994).

Although the freshening-induced large cooling events occured during cold climates, sensitivity studies with coupled circulation models (e.g. Manabe and Stouffer, 1995, 1996; Schiller et al., 1996) simulate melt water events to the current interglacial rather than the last glacial. One aim of this paper is to analyze the role of the background climate on the ocean's sensitivity to fresh water input. For this purpose, we analyze the climate model of Lohmann et

al. (1996 b) which is based on Stommel's model.

Besides the paleoclimatic shifts, interdecadal climate variability may originate from changes of North Atlantic Deep Water (NADW) formation. A large salinity fluctuation in the northern North Atlantic was observed in the late sixties/early seventies, known as the "Great Salinity Anomaly" (Dickson et al., 1988; Reverdin et al., 1994) which temporarily weakened deep water formation in the Labrador Sea (Lazier, 1988). A fresh water anomaly developed in the Greenland-Iceland-Norwegian Sea and moved southward passing the regions of deep water formation. It has been suggested that the Great Salinity Anomaly originated from atmosphere-ocean interactions (Dickson et al., 1988).

In order to detect the effect of anthropogenic greenhouse warming, the understanding of such variability is an important issue. Up to now, modelers have not a consistent picture to understand the interdecadal climate variations related to the THC. What they can do, is to analyze possible mechanisms leading to variability in different models (see for a recent review: Stocker, 1996). Some examples of interdecadal modes simulated in coupled models are given by Delworth et al. (1994), Griffies and Bryan (1997 a, b), and Timmermann et al. (1997).

One may ask why salinity perturbations affect strongly the THC, and if long-term climate variations are linked to fluctuations in high latitude sea surface salinity. In our simple coupled model, we separate the density contribution of salinity and temperature and find that sea surface salinity anomalies are of great importance affecting the THC.

Although the typical predictability limit of weather phenomena is of the order of about weeks, climate variations are much more predictable due to the ocean's large heat capacity and dynamical interia. The question of the atmosphere's predictability started with the work of Lorenz (1965). This was later extented to a coupled atmosphere-ocean mixed layer model (Nese and Dutton, 1993). Other modeling studies deal with the forecast of the dominant interannual climate fluctuation, the El Niño/Southern Oscillation (Goswami and Shukla, 1991; Blumenthal, 1991; Eckert and Latif, 1997). For the North Atlantic, predictability studies include an active THC which was recently addressed by Griffies and Bryan (1997 a, b).

Griffies and Bryan (1997 b) show that the leading empirical orthogonal functions (EOFs) of the surface fields contribute mostly to the multidecadal variability whereas higher EOFs have a neglible amount. In several predictability experiments with their complex coupled model, they estimated the predictability of these dominant patterns. They concluded that the ocean-atmosphere interaction lead to predictability limits beyond the intrinsic predictability limit of the atmosphere. Their finding that the dynamics of their high dimensional model can be reduced to a few statistical modes, encourages us to investigate the error growth dynamics in our simple coupled box model.

Our model mimics the North Atlantic region which seems to be a very sensitive part of the global thermohaline circulation. In our model study, we concentrate on the northern source of the THC and deliberately exclude any source of southern hemisphere forcing and the interaction of the THC with wind.

We present the analytical solution of Stommel's (1961) low order model. Along with our coupled atmosphere-ocean version of Stommel's model, we analyze the qualitative behavior of the THC in terms of stability, variability, and predictability.

Stability is understood here in the sense of Lyapunov:
If the initial condition is in the attractor of an equilibrium state, the system reaches a neigbourhood of the equilibrium at finite times. The attractor can be obtained by the Lyapunov function technique or by the direct solution of the dynamical system. Under the system's sensitivity, we understand a parameter dependence of the stability properties. One particular interest here is the most effective initial perturbation maximizing the response in our system.

The *variability* of dynamical system can be explored by several concepts:
- The model may undergo a limit cycle or a more complex attractor which implies at least one dominant negative feedback in the system.
- The model is forced by external forcing such as variations in solar activity.
- The system has two different inherent time scales, where the short-period component lead to a response of the slower component (Hasselmann, 1978).
Variability is understood here as the amount of stationary variance of the

dynamics. Our coupled box model is forced by stochastic atmospheric white noise which stems in turn from the underlying dynamical processes in the atmosphere. We are particularly interested in the type of forcing which leads to maximal long-term variance.

The *prediction* of a process provides information how small perturbations in the initial conditions cause significant changes in the subsequent evolution. In our context, we define the predictability as the error growth amplification and as the evolution of the probability distribution function in phase space.

The paper is organized as follows:

We present the exact solution of the nonlinear differential equations with quadratic nonlinearity of Jacobi-type in section 2. We show that Stommel's (1961) box model falls into this class and give the solution of a coupled version of this model. The critical perturbation in sea surface salinity inducing a break down of the model's THC is calculated.

In section 3, the box model's dynamics are analyzed with respect to the forecast properties and the most effective excitation of the model. These concepts are used to understand the coupled box model's climate variability and error growth dynamics. In section 4 we analyze, how the THC's stability is affected by the background climate.

Section 5 deals with a coupled energy balance-ocean circulation model. We analyze the feedbacks and compare the results with the sensitivity in the box model. The conclusions are given in section 6.

2 A simple climate model

In this section, a category of the nonlinear models following Stommel's (1961) ansatz is solved exactly and the feedbacks affecting the THC are analyzed. The common assumption of Stommel (1961)-type box models is that the oceanic overturning rate Φ can be expressed by the meridional density difference:

$$\Phi = -c(\alpha\Delta T - \beta\Delta S) \quad , \tag{1}$$

where α and β are the thermal and haline expansion coefficients, c is a tunable parameter, and Δ denotes the meridional difference operator. The equations for temperature T and salinity S are the heat and salt budgets in one oceanic box using an upstream scheme for the advective transport:

$$\frac{d}{dt}T = -\frac{\Phi}{V}\Delta T - \frac{F_{oa}}{\rho_0 c_p h} \tag{2}$$

$$\frac{d}{dt}S = -\frac{\Phi}{V}\Delta S - \frac{S_0}{h}(P-E) \quad , \tag{3}$$

where V is the volume of the box with depth h, $(P-E)$ denotes the fresh water flux (precipitation minus evaporation plus runoff). F_{oa} is the heat flux at the ocean-atmosphere interface, S_0 is a reference salinity, and $\rho_0 c_p$ denotes the heat capacity of the ocean.

For simplicity, we have restricted our notation to the case with high latitude deep water formation and do not consider the equilibrium with sinking water at low latitudes. In the solution of these types of models, the variable $(\Delta T, \Delta S)$ consists of the components to the meridional buoyancy gradient.

2.1 Exact solution of Stommel's model

Schneider and Lohmann (1997) solve a class of nonlinear evolution equations of the following structure:

$$\frac{d}{dt}X = AX + < b \mid X > X, \qquad X(0) = X_0 \in \mathsf{R}^n \tag{4}$$

for $X \in \mathsf{R}^n$, $n \in \mathsf{N}$. The brackets $< \mid >$ denote the euclidian scalar product. The vector b and linear operator A are arbitrary as long as there exists a solution $\xi \in \mathsf{R}^n$ for

$$A^*\xi + b = 0 \quad , \tag{5}$$

where A^* denotes the adjoint operator to A. Equation (4) is solved with a transformation to the linearized evolution equation. With the definition

$$X(t) := \frac{1}{\gamma(t)} \exp(At)\, X_0 \ , \qquad X_0, X(t) \in \mathsf{R}^n \tag{6}$$

and the scaling function

$$\gamma(t; X_0) := < \xi \mid \exp(At) X_0 > \ - \ < \xi \mid X_0 > \ + 1 \quad , \tag{7}$$

one can verify that $X(t)$ solves the differential equation (4):

$$\begin{aligned} \frac{d}{dt} X &= A \frac{1}{\gamma} \exp(At) X_0 \ - \frac{\dot{\gamma}}{\gamma^2} \exp(At) X_0 \\ &= AX - < \xi \mid AX > \ X \ = \ AX + < b \mid X > \ X \ . \end{aligned} \tag{8}$$

The evolution (6) is defined for times t as long as $\gamma(t; X_0) > 0$. How this solution and that of the corresponding partial differential equation are obtained, is described in a proper mathematical context in Schneider and Lohmann (1997).

The models of Stommel (1961), Marotzke and Stone (1995), Lohmann et al. (1996 b), Ruddick and Zhang (1996), Winton (1997) and many others are of the type of equation (4), and their dynamics are therefore exactly known. For two-box ocean models, as e.g. Stommel (1961), the budget equations for temperature and salinity (2, 3) for each box with volume V can be subtracted from each other to get the form (4):

$$\frac{d}{dt}\Delta T \ = \ -2 \ \frac{\Phi}{V} \Delta T \ - \ \Delta \frac{F_{oa}}{\rho_0 c_p h} \tag{9}$$

$$\frac{d}{dt}\Delta S \ = \ -2 \ \frac{\Phi}{V} \Delta S \ - \ \Delta \frac{S_0}{h}(P - E) \quad , \tag{10}$$

We proceed with the notation of the Lohmann et al. (1996 b)-model which is based on the Stommel's ocean model and the linearized atmospheric energy balance model of Chen et al. (1995). This model consists of two boxes for the upper ocean and two boxes for the atmosphere. The geometry of the model (figure 1) mimics the North Atlantic, with an ocean box at low latitudes ranging from the equator to 40^0 N, a high latitude box between 40^0 and 70^0 N, and one ocean box for the deep ocean. Both upper ocean boxes are 100 m thick. This three-box model is of the type (4) after introducing a climatological background state with meridional temperature and salinity gradient, ΔT° and ΔS°, respectively. The model is tuned for the present

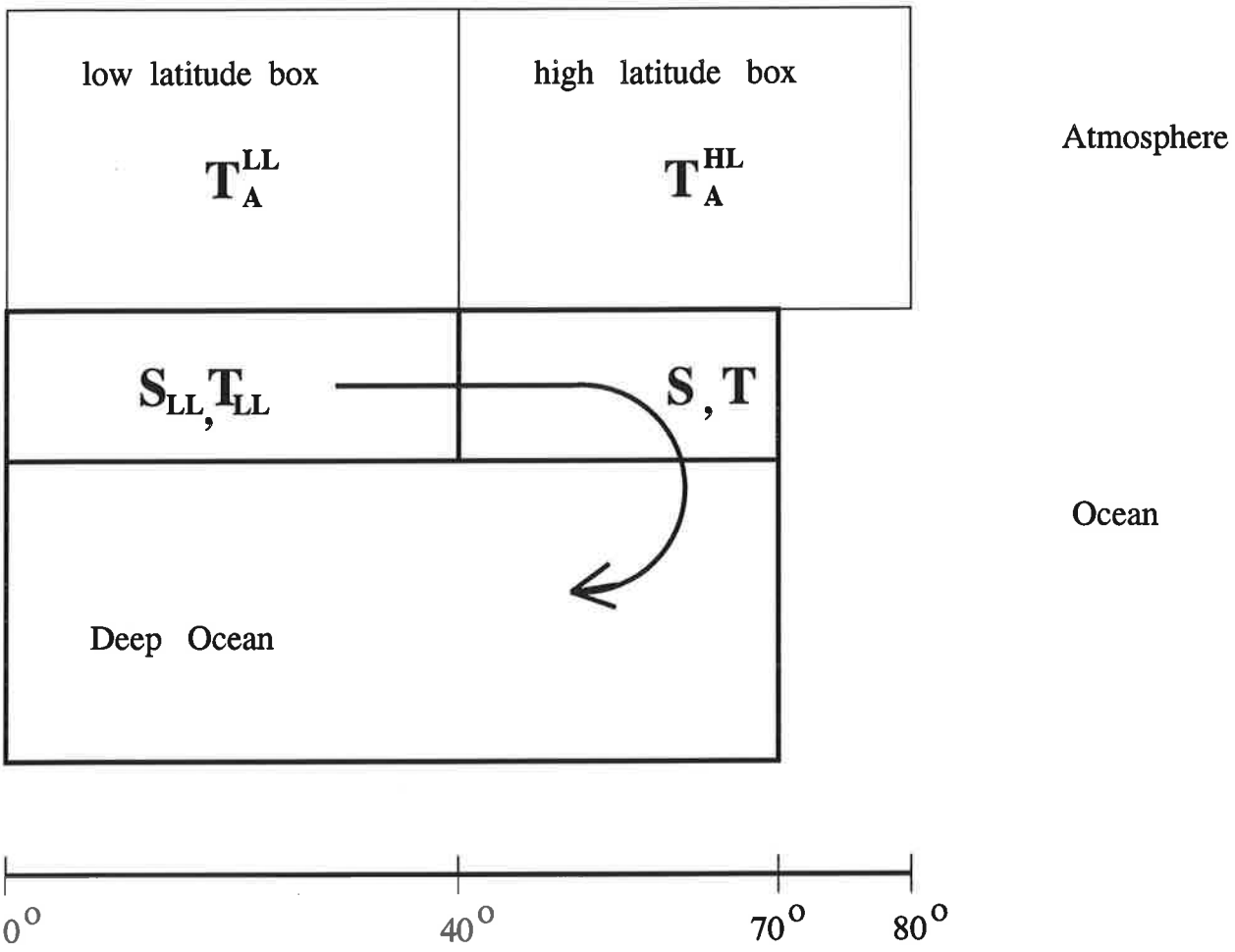

Figure 1: Schematic representation of the box model's configuration.

climate which places it in the thermal regime of the THC (Lohmann et al., 1996 b).

The atmosphere is vertically integrated and consists of a low latitude box ranging from the equator to 40^0 N and a high latitude box between 40^0 N and 80^0 N. The heat flux at the ocean-atmosphere interface is parameterized linearly as

$$F_{oa} = Q_1 + Q_2 \, (T_A - T) \tag{11}$$

with fixed values for Q_1 and Q_2 and sea surface temperature T and atmospheric temperature T_A at 1000 mb. The atmospheric part of the model is a linear response model where the eddy fluxes in the atmospheric model are parameterized as diffusion. The fresh water flux $P - E$ is equal to the divergence of vertically integrated water vapour transport. In the atmospheric transport model, the anomalous heat and fresh water balances are related to the change of meridional temperature gradient δT_A:

$$K \;\; \delta T_A \;\; = \;\; Q_2 \;\; \delta \, (T_A - T) \;\; - \;\; B \;\; \delta T_A \tag{12}$$

$$K_2 \;\; \delta T_A \;\; = \;\; \delta \, (P - E) \;\; , \tag{13}$$

where K and K_2 denote the coefficients for the atmospheric heat transport which are estimated to be $7.2 \, W \, m^{-2} \, K^{-1}$ and $40 \, mm \, yr^{-1}$ (Lohmann et al., 1996 b). B is the coefficient for long wave radiation change ($B = 2 \, W m^{-2} K^{-1}$). For the thermal response, a parameter ϵ is introduced. This parameter accounts for changes of the atmospheric surface temperature compared to changes in sea surface temperature:

$$\epsilon = \frac{\delta T_A}{\delta T} = \frac{Q_2}{Q_2 + B + K} \;\; . \tag{14}$$

The dynamics of the model is known, when the vector $\xi = -(A^*)^{-1} \, b$ of equation (5) is specified:

$$\xi = \frac{\begin{pmatrix} c\alpha\Phi^\circ - c\beta \, \epsilon \, K_2 \, S_0 V/h \\ c\beta\Phi^\circ + c\beta q_2 (1 - \epsilon) \end{pmatrix}}{-2\Phi^\circ\Phi^\circ + (c\alpha\Delta T^\circ - 2c\beta \, \Delta S^\circ) \; q_2(1 - \epsilon) - c\beta \, \Delta T^\circ \, \epsilon K_2 S_0 V/h} \;\; , \tag{15}$$

where q_2 is an abbreviation for $Q_2 \, V/(\rho_0 c_p h)$. The denominator in (15) is the negative of matrix A's determinant. The units of vector $\xi = (\xi_1, \xi_2)$ are $1/K$ and $1/psu$, respectively. For mixed boundary conditions, as e.g. in Stommel's (1961) model, the atmospheric temperature and fresh water flux are fixed. In this case, the parameters ϵ and K_2 are therefore set to zero.

2.2 Critical salinity perturbation

The critical salinity perturbation causing a breakdown of the thermohaline circulation is considered by means of the above exact solution. This question can be reduced to the determination of the time interval where the solution $X(t)$ exists. By definition, $\gamma = 1$ initially. If $\gamma(t; X_0) > 0$ for all $t \geq 0$, the dynamical system (6) with initial condition X_0 is stable. An analysis shows that the sign of γ is affected by the last two terms in (7) only, if we assume salinity perturbations as initial conditions $X_0 = (0, -S_{crit})$ in our box model. The critical perturbation $S_{crit} > 0$ is:

$$S_{crit} = \frac{1}{\xi_2} \quad . \tag{16}$$

With perturbations smaller than S_{crit}, the system recovers and returns to its basic state. With perturbations larger than S_{crit}, the system goes into another climate state with low latitude sinking. For $t \geq t_1$, the parameter c in (1) must then be substituted by $-c$ (Stommel, 1961). Here, we analyze only the high latitude sinking solution of the model and exclude deliberately the bifurcation problem in the context of multiple equilibria (as e.g. in Ruddick and Zhang, 1996; Rahmstorf, 1996). Equation (16) is analyzed with respect to the atmospheric response model (section 2.3) and the basic state (section 4).

2.3 Uncertain atmospheric response

There are great uncertainties of the atmospheric thermal and fresh water flux response. Our model and other simplified energy balance models (Chen et al., 1995; Rahmstorf and Willebrand, 1995) assume a negative thermal feedback (damping SST-anomalies), whereas some other studies found a positive feedback (Palmer and Sun, 1985; Latif and Barnett, 1994). The atmospheric response to mid and high-latitude SST anomalies is, however, still a highly controversial issue.

Furthermore, there are large uncertainties in estimating changes in the hydrological cycle. For example, it is not clear whether today's fresh water export from the North Atlantic (Zaucker and Broecker, 1992; Wijffels et al., 1992) will change under different climate conditions. An enhanced export would stabilize the THC in contrast to the anomalous meridional water vapor transport. The geographic location of changed precipitation, evaporation

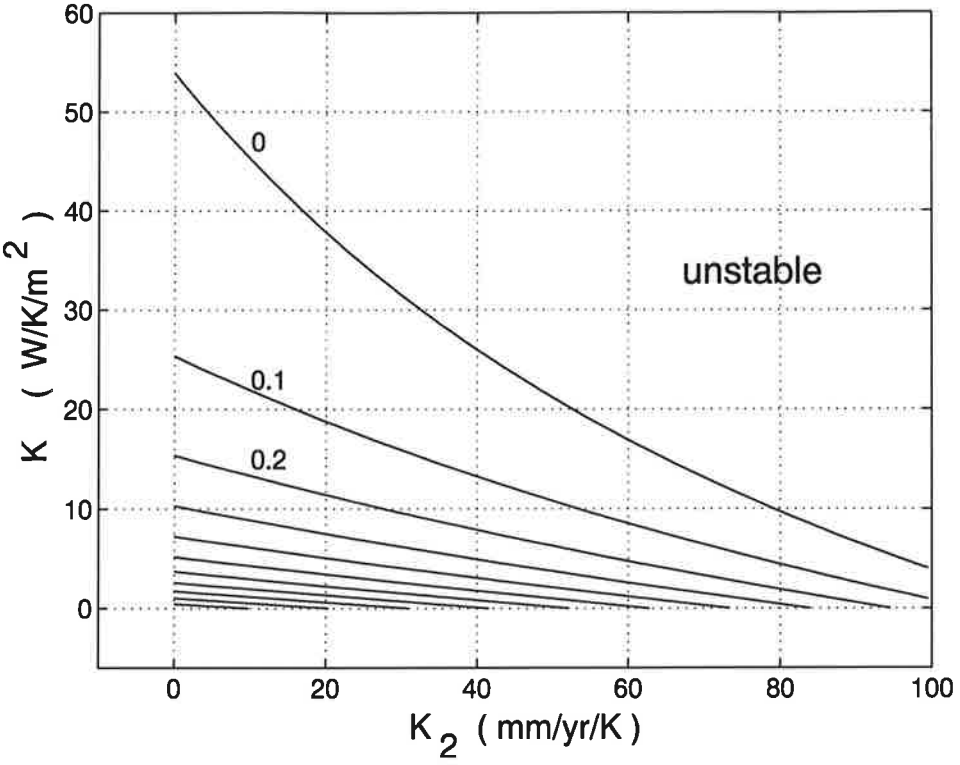

Figure 2: Critical salinity perturbation for the coupled system in the parameter space for the eddy coefficient of heat transport K and the sensitivity coefficient of the hydrological cycle K_2. The contour interval for S_{crit} is 0.1 psu. The coupled system is unstable above the curve $S_{crit} = 0$.

and runoff may furthermore influence the sensitivity of the THC.

Therefore, we calculate the critical perturbation (16) as a function of the hydrological feedback K_2 and the thermal feedback K (figure 2). K is the meridional heat flux rate by transient eddies. Small numerical values of (K_2, K) indicate a small response of the atmosphere to changes in the ocean. For small K_2 and K, the critical perturbation S_{crit} is rather large (figure 2). For larger values, the coupled system becomes more unstable. Negative S_{crit} indicate an unstable THC where the curve $S_{crit} = 0$ coincides with the line of neutral stability in the linear stability analysis (Lohmann et al., 1996 b, figure 2 therein).

The solution of the coupled model shows how the assumed strengths of the atmospheric heat transport and freshwater flux determine the critical salinity perturbation. Mixed boundary conditions with fixed atmospheric temperature and fresh water flux correspond to $\epsilon = 0$ (or $K = \infty$) whereas an

ocean model with fixed surface fluxes to $\epsilon = 1$ (or $K = 0$). Therefore, the atmospheric transport feedbacks affect strongly the stability of the thermohaline circulation.

Lohmann et al. (1996 a) look for the THC's equilibrium response using various upper boundary conditions for an ocean circulation model. They conclude that multiple equilibria are not possible when using an atmospheric model with small K_2 and K, and conclude that such models provide for a too strong constrain for the coupled atmosphere-ocean system whereas mixed boundary conditions (corresponding to a very large K) overestimate the possible existence of multiple equilibria.

The question of adequate transport coefficients K and K_2 hints to the question of the proper boundary conditions for ocean sensitivity experiments. In principle, the slow parts of a system can be considered as prescribed boundary conditions to the more mobile one to simulate climate variations at a specific time scale. Therefore, there is still a controversial debate about the proper boundary conditions for ocean sensitivity experiments. Sensitivity studies with coupled general circulation models are too costly for computers of the present generation. Asynchronous integration techniques used to reduce the computer time required in coupled GCM integrations cannot circumvent this problem, because such integrations may not provide the correct feedbacks during the ocean only phase.

Each set of upper boundary conditions used implies an own atmospheric model. In contrast to atmospheric studies with fixed SST as a relatively persistent quantity to perform parameter sensitivity, the ocean's sensitivity is not known in a coupled context, because the parameter sensitivity of ocean-only models may not give the correct insight in that of a coupled model. In a recent parameter study, Weber (1997) shows that the sensitivity of the oceanic circulation with respect to subgrid-scale parameters, such as the vertical diffusivity, is strongly affected by the boundary conditions or the kind of atmospheric model used.

We shall see in section 3.4 that long-term climate variability must be seen in the coupled atmosphere-ocean context rather than in a so called "ocean-only mode". In section 5, we will compare the response to sea surface salinity anomalies in the box model to that of a more complex model.

3 Optimal response analysis

In this section we analyze the box model's sensitivity and variability. In particular, we examine why salinity perturbations are so important in changing the THC. Furthermore, the predictability of the model is investigated using the error growth analysis. We make use of the generalized stability theory of non-normal operators, recently proposed by Farrell and Ioannou (1996) and Palmer (1996). Throughout this section, we restrict our examination to the current climate. In section 4, we discuss the dynamics for different climatic states.

3.1 Regimes after a salinity perturbation

We analyze the time regimes of $X(t)$ in the phase space spanned by salinity and temperature anomalies. As in section 2.3, we investigate the box model's sensitivity under anomalous high latitude haline forcing as an initial perturbation. The solid line in figure 3, denoted as b), is the phase space trajectory of the system's response to a negative salinity perturbation at high latitudes for the present climate (Lohmann et al., 1996 b). The phase space trajectory shows a decrease in temperature for the first 5 years, where the distance of the trajectory from zero point increases temporarily. After about 10 years the trajectory in figure 3 points into a "mixed temperature/salinity direction", denoted further as e_1. Our results imply that the adjustment of the THC involves two phases: A fast thermal response and a slower response on the e_1-direction.[1]

Because the fast response is associated with temperature anomalies only (figure 4), a rapid cooling takes place after a perturbation in salinity (not in temperature) is introduced into the system. This is consistent with our picture obtained from paleo data of rapid temperature changes occurring after high latitude freshening (Dansgaard et al., 1993). For the THC, this is a stabilizing effect: A negative salinity perturbation accounts for a negative temperature anomaly increasing the high latitude density.

The evolution of the nonlinear model can be characterized well with the eigenvectors of the matrix A, because the scaling function $\gamma(t)$ acts upon both temperature and salinity (equation 6). This is done in section 3.2 where

[1] We shall see later that e_1 is identical with the most unstable mode in the system.

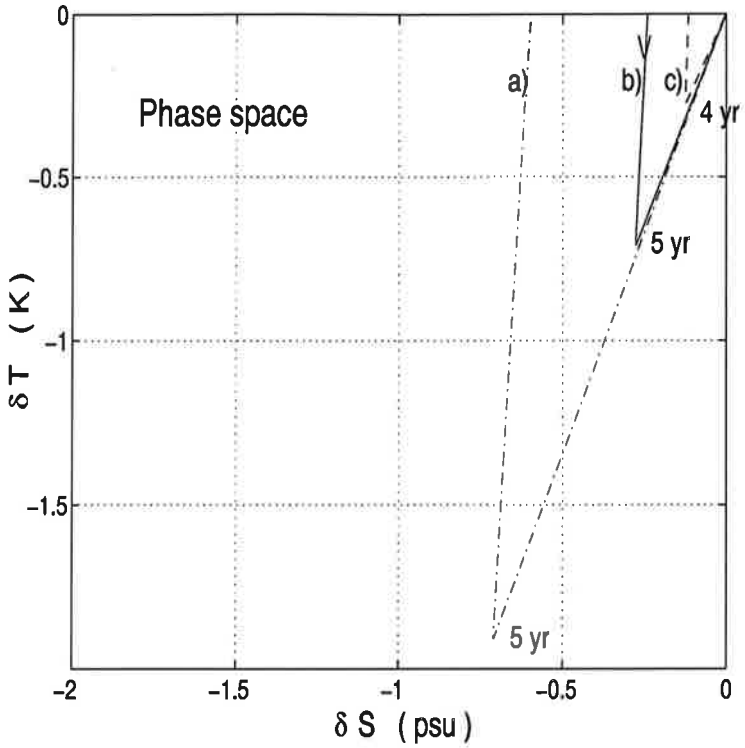

Figure 3: The dynamics in the thermo-haline phase space after a salinity anomaly. The different climatic states a), b), c) are listed in table 1.

we examine that high growth rates can occur over intermediate times even though both eigenmodes are damped.

3.2 The biorthogonal vector: Initial excitation

Our dynamical system (4)

$$\frac{d}{dt}X \quad = \quad f(X) \qquad , \qquad \text{with } X \in \mathsf{R}^2 \tag{17}$$

has the tangent linear operator $A(X)$ on the tangent vector space with evolution x:

$$\frac{d}{dt}x \quad = \quad \frac{df}{dX}(X) \quad x \quad = \quad A(X)\, x \qquad . \tag{18}$$

In our box model, the evolution $X(t)$ is known. Thus, $A(X)$ can be obtained analytically.

The operator A of the box model is found to be non-normal $(AA^* \neq A^*A)$, the eigenvectors of A, and e_1 and e_2, are not orthogonal (figure 4). One eigenvalue (e_2) is closely related to temperature anomalies, whereas the other (e_1) is a "mixed temperature/salinity eigenvector" (figure 4). The eigenvectors of the adjoint matrix A^* are denoted by e_1^* and e_2^*, respectively.

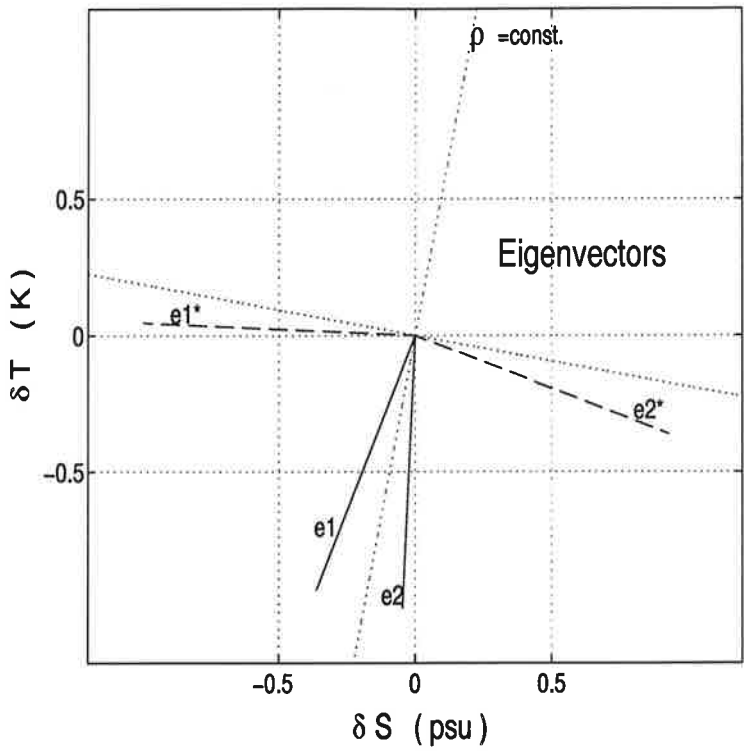

Figure 4: Eigenvectors e_1, e_2, and adjoint eigenvectors e_1^*, e_2^* of the tangent linear operator A for the present climate. The dotted lines show the line of constant density and the perpendicular.

For the non-normal matrix A, the eigenvectors of A and A^* do not coincide. However, the eigenvectors of A and A^* are perpendicular to each other, fulfilling the "biorthogonality condition":

$$e_i^* \perp e_j \quad \text{for} \quad i \neq j \quad . \tag{19}$$

For the linear dynamics of x, we make the ansatz

$$x \quad = \quad c_1 \, \mathbf{e_1} \, \exp(\lambda_1 t) + c_2 \quad \mathbf{e_2} \quad \exp(\lambda_2 t) \quad , \tag{20}$$

where eigenvalue λ_1 corresponds to the most unstable eigenvector e_1 and λ_2 is the eigenvalue to the temperature eigenvector e_2. Multiplying (20) with e_1^* and e_2^* for initial time and using condition (19), we get the coefficients

$$c_i = \frac{< e_i^* \mid x_0 >}{< e_i^* \mid e_i >} \qquad \text{for} \quad i = 1, 2 \quad . \tag{21}$$

In our system, both eigenvalues are real and negative. Because of $\lambda_2 < \lambda_1$, the first term dominates for long times and the second for small times.

A perturbation is called "optimal", if the initial error vector projects onto the most growing subspace. It follows from (20) that the coefficient c_1 for the most unstable mode must be maximal. This is according to (21) equivalent

with that x_0 points into the direction of e_1^*. Note, that vector e_1^* is closely related to salinity anomalies of the high latitudinal box.

This unit vector e_1^* is called the "biorthogonal" to the most unstable eigenvector e_1 which we want to excite. In order to make a picture for the mathematical considerations, we assume that the tail of x_0 is placed on the e_1-line and its tip on the e_2-line. This vector is stretched maximally because the tail decays to zero quickly, whereas the tip is hardly unchanged due to the larger eigenvalue λ_1.

It is remarkable that the optimal initial perturbation vector x_0 does not coincide with a perturbation in sea surface density at high latitudes which would reside on the dotted line perpendicular to $\rho = const.$ in figure 4. Even when using a space spanned by $(\alpha T, \beta S)$ instead of (T, S) to take into account the different values for the thermal and haline expansion coefficients, vector e_1^* is much more dominated by the scaled salinity anomalies than for temperature anomalies of the high latitudinal box. We have chosen the (T, S)-space instead of $(\alpha T, \beta S)$, in order to make the phase space analogy more clear and to discuss the effect of changed α under different climatic conditions (section 4).

Our investigation of the most efficient initial excitation of the THC supports the picture that the choice of proper boundary conditions is essential for modeling the system's qualitative behavior: The ocean model (2, 3) with fixed fluxes (with $K_2 = 0$, $K = 0$) can be reduced to a single density equation. This would imply, the most efficient perturbation would be a sea surface density anomaly at high latitudes. The non-normality reflects therefore the system's different timescales: Sea surface temperature anomalies are quickly damped whereas sea surface salinity anomalies can persist longer. Here, in our two dimensional system, the most unstable mode e_1 and its biorthogonal e_1^* differ greatly from each other, and the perturbation that optimally excites the mode bears little resemblance to the mode itself.

This might explain the THC's sensitivity to perturbations in high latitude salinity, which has been observed in the northern North Atlantic for the recent (Lazier, 1988) and the past climate (Bond et al., 1993). The initial error is most efficient when the projection of the perturbation onto salinity is large, and the transient growth is almost entirely due to the temperature

adjustment on short time scales.

3.3 The error growth: Forecast ellipsoid

Let us investigate the linear stage of the dynamics in order to obtain some insight into the predictability of the system. The evolution on the tangent vector space is given by

$$x(t) = \exp(At)\ x_0 \ =: \Psi\ x_0 \qquad , \tag{22}$$

defining an evolution operator Ψ on the tangent vector space $T_X\mathsf{R}^2$. Unlike Ψ itself, the operator $\Psi^*\Psi$ is symmetric and provides a measure for the error growth. The eigenvectors of $\Psi^*\Psi$ are called singular vectors. They define the axes of the forecast ellipsoid for the probability distribution function. The corresponding eigenvalues are called the singular values σ_1, σ_2. Here, we analyze the error growth with respect to the euclidic norm because our model contains only the kinetic energy (proportional to Φ^2) as a basic quantity.

Supposing that an error/uncertainty in the initial conditions is represented by a normally distributed probability distribution function. This function is represented by a circle in phase space (figure 5) where the axis units correspond to the same density contribution. The development of the forecast ellipsiodes is shown in figure 5 for five different times: 1 day, 1 month, 6 months, 1 year, and 2 years. The circle is stretched during the evolution thereby decreasing its volume by the factors $0.99, 0.89, 0.50, 0.25, 0.06$, respectively. The main axes of the ellipsoids define the singular vectors of the system. On the tangent vector space, the error growth is along the most unstable singular vector. Initially, $\Psi^*\Psi$ can be traced by a Taylor expansion:

$$\Psi^*\Psi = \mathbf{1}\ +\ (A^* + A)\ t\ +\ o(t^2) \qquad .$$

Thus, the dominant singular vector for initial time coincides with the vector $(e_1 + e_1^*)/2$ and can be obtained from e_1 and e_1^* in figure 4. After one year, the dominant singular vector coincides almost with sea surface salinity anomalies. We obtain that ellipsoids after few years degenerate to a line, and asymptotically they are reduced to the origin $(0, 0)$ because the matrix A is stable. However, the error growth dynamics $\Psi^*\Psi$ on the tangent vector space $T_X\mathsf{R}^2$ is then no longer valid, and the nonlinear terms have to be taken into account.

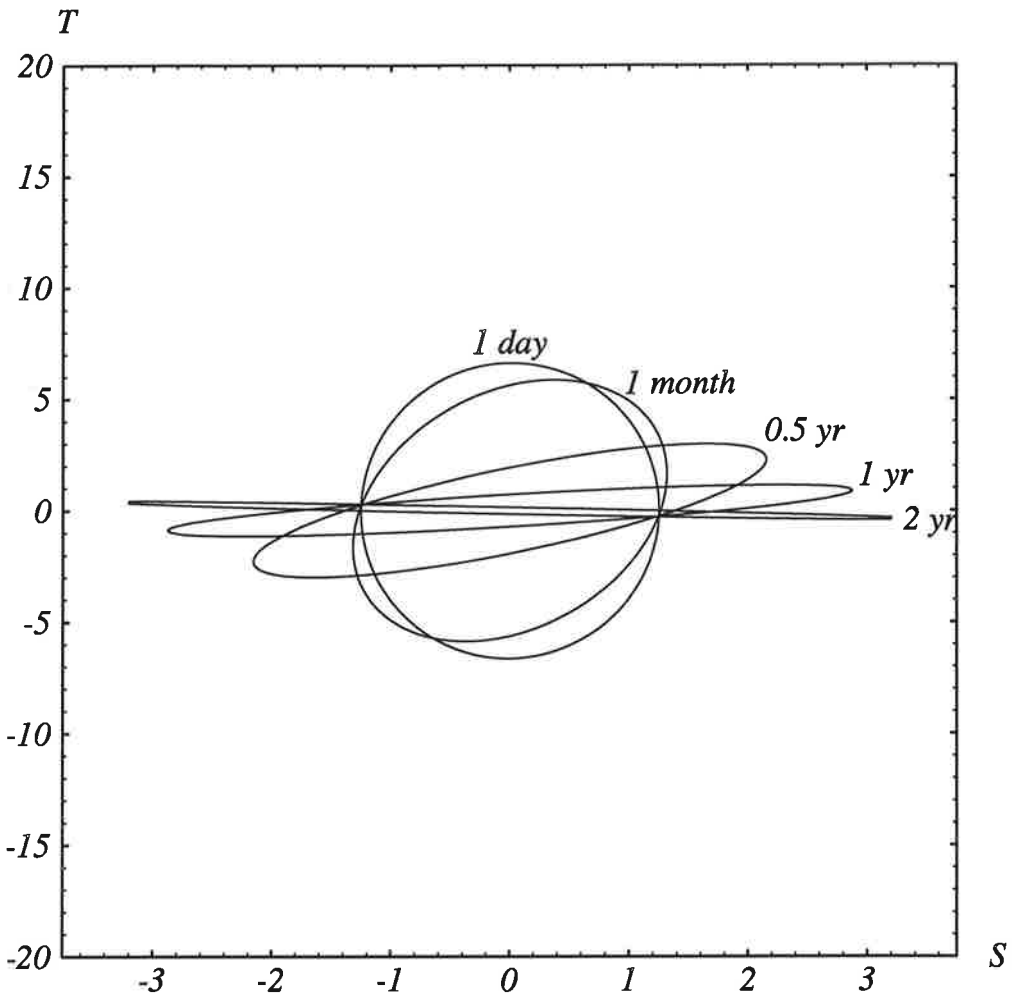

Figure 5: Forecast ellipsoid after 1 day, 1 month, 6 months, 1 year, and 2 years. The main axes of the ellipsiodes define the singular vectors of the system. After a year, the dominant singular vector coincides allmost with sea surface salinity anomalies. The axes are scaled for equal contributions of salinity and temperature to high latitude density.

It follows that high latitude sea surface temperatures (SST) are much more predictable than sea surface salinities (SSS). Our explanation is that the atmospheric feedbacks damp strongly temperature anomalies which thins down the forecast ellipsoid. In our buoyancy driven model of the THC, the time necessary to transport low latitude warm surface waters to high latitudes is longer than that for the local temperature effect. Salinity on the other hand is dominated by the slow advective processes. The positive feedback due to salinity advection, destabilizing the THC, increases the error growth further.

We find that a negative feedback (damping) of SST-anomalies in the northern North Atlantic is essential for our conclusions. The time scales of the amplifications of the standard deviations along the directions of singular vectors are very different. Increasing the restoring times in the heat flux parameterization, the forecast ellipsoid becomes therefore more spherical. We find furthermore that the dominant error growth vector changes only slightly for different background climatic states and thus for a whole model trajectory $X(t)$.

Often, Lyapunov exponents are used to quantify the time averaged predictability. The mean growth rate is given with the Ergodic theorem of Oseldec (1968) defining Lyapunovnumbers $\lambda_{1,2}$, which are global characteristica of the dynamical system:

$$\lambda_i := \lim_{t\to\infty} \frac{\ln \parallel A(X_t)x \parallel}{t} = \lim_{t\to\infty} \frac{\ln \sigma_i}{t} \quad , \tag{23}$$

where the second equation relates the singular values to the Lyapunov exponents. The sum of the Lyapunovnumbers is related to the divergence rate of (18) averaged over the stationary probability distribution function. We prefer singular values instead of Lyapunovnumbers because they quantify only time averaged predictability and do not take the transient growth into account. Similarly to the singular vector analysis, one can describe the predictability by local divergence rates within the framework of dynamical system theory (e.g. Lorenz, 1965; Nese and Dutton, 1993).

3.4 Stochasic optimals: Maximal variance

In the previous sections 3.2 and 3.3, we have looked for the sensitivity of the THC with respect to initial conditions. In contrast, we are interested

here how the system responds to changes in some external forcing which is interpreted as an uncertainty in the model formulation. In the long-term predictability problem, the error growth arises from an ensemble of growing perturbations that are excited. We want to look at the statistically steady state, and investigate that permanent perturbation which most effectively excites the stationary variance. Furthermore, we look for the eigenvectors which span the maintained variance, commonly referred as to the empirical orthogonal functions (EOFs).

We generalize (18) to the stochastically driven, linearized dynamical system

$$\frac{d}{dt}x \quad = \quad A\,x \; + F\,\eta_t \quad , \qquad x, \eta \in \mathsf{R}^2 \tag{24}$$

with η_t a white-noise forcing. The additive noise reflects the very different time scales of ocean and atmosphere (Hasselmann, 1976): Large-scale atmospheric fluctuations in the meridional transport processes are integrated by the slower component, the ocean. Different realisations of the atmospheric response are modelled as random heat and fresh water flux in the components of η_t. A similar approach was used by Eckert and Latif (1997) studying ENSO predictability.

The analytical solution of the linear stochastic differential equation (24) is

$$x(t) = \int_o^t e^{A(t-s)}\, F\, \eta_s \, ds \qquad . \tag{25}$$

As in Farrel and Ioannou (1996), the spatial distribution of the forcing is assumed to be represented by an unitary F, such that the resulting statistics become independent of the particular choice of F.

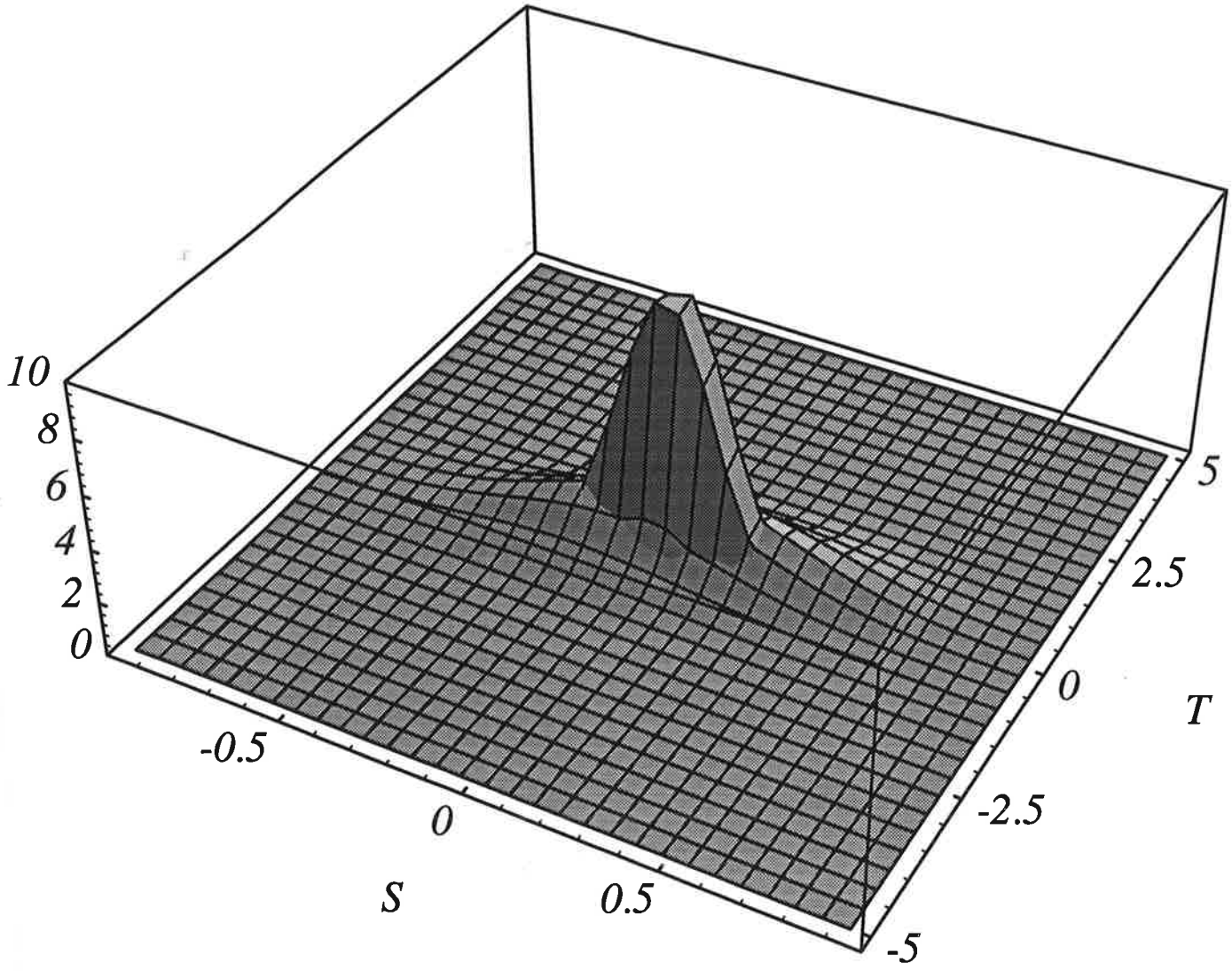

Figure 6: Development of the probability distribution function (PDF). Starting with a $\delta-$function, the PDF is shown after one month together with the PDF for six months. The axes are scaled for equal contributions of salinity and temperature to high latitude density.

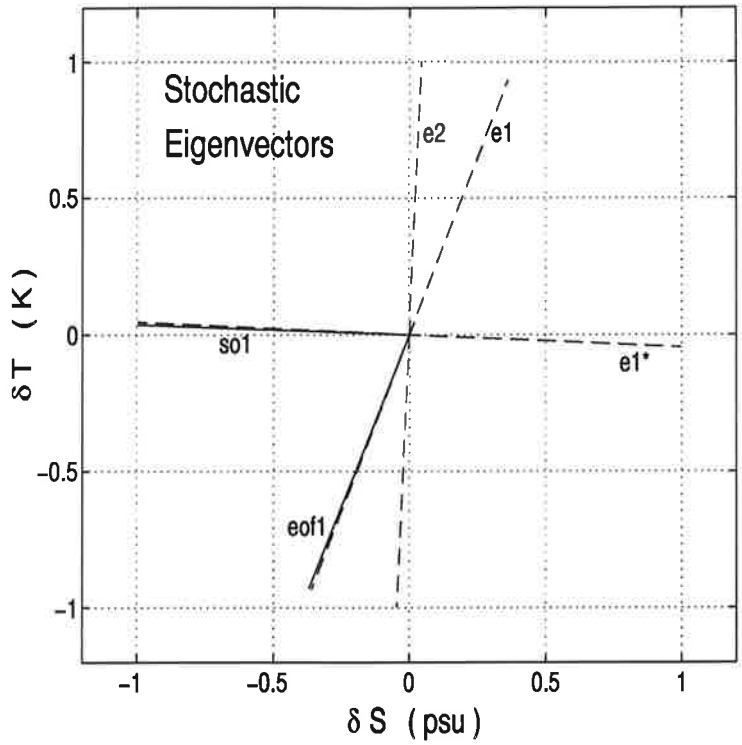

Figure 7: The first EOF (eof1), the stochastic optimal (sol). For orientation, the direction of eigenvectors e_1, e_2 and adjoint eigenvector e_1^* are shown with dashed lines.

We use an F such that the stochastic forcing components have equal contributions to the high latitude density. The solution (25) corresponds to the solution for a Fokker-Planck equation, an evolution equation for the probability distribution function (PDF). Starting with a $\delta-$function at initial time, the PDFs for one month and six months are plotted together in figure 6. The variance increases in time and the figure shows furthermore that sea surface salinity has a much larger variance compared to sea surface temperature. Thus, the system's response to an external forcing shows a similar behaviour as the error growth dynamic on the tangent linear vector space, conducted by the singular vector analysis in section 3.3. However, the PDF-prediction is by construction not sensitive to initial conditions, because the initial conditions are exactly known. Uncertainties/error growth of the initial conditions further limit the system's predictability and are largely affected by the model's nonnormality (section 3.3). In contrast, the stochastic approach (24) measures the knowledge of the system's variance. The stationary PDF has maximal variance and contains therefore less information about the system. Thus, unpredictability can be associated with the overlap of the actual PDF with the stationary PDF (Eckert and Latif, 1997).

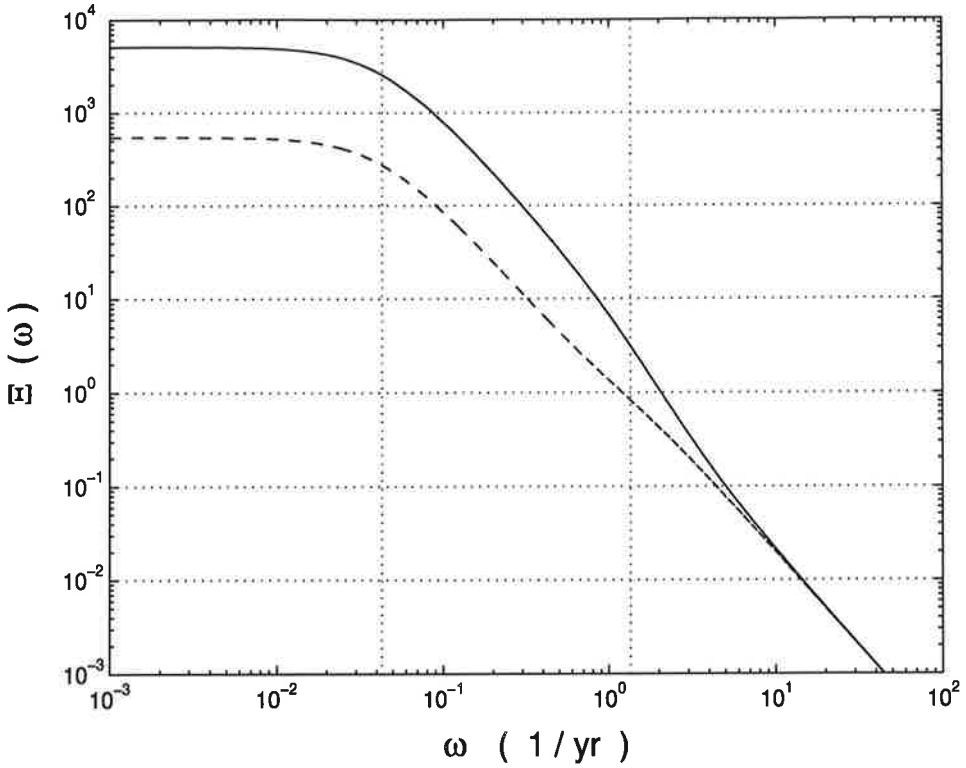

Figure 8: Ensemble response variance (solid line) compared with the ensemble response variance for a system with orthogonal eigenvectors (dashed line). The dotted lines in the vertical show the eigenfrequencies $1/\lambda_1 = 0.0431/yr$ and $1/\lambda_2 = 1.351/yr$, respectively.

In the following, another aspect of the stochastic dynamics (24) is discussed. We seek for the stochastic forcing F which gives maximal variance of the stationary solution. From (25), the variance maintained by the stochastic forcing is

$$\begin{aligned} Var(x) &= E\left\{x^2\right\} = Trace\left[F^* \left(\int_o^t e^{A^*(t-s)}\, e^{A(t-s)} ds\right) F\right] \\ &= Trace\left[F^*\, B_t\, F\right] \end{aligned} \tag{26}$$

with the positive hermitian B_t accumulating the perturbation growth. The variance (26) is maximal, if the matrix F consists of the eigenvectors of B_t, because then the matrix $F^*\, B_t\, F$ has diagonal form and the trace is maximal.

Because the matrix A is asymptotically stable, the statistics are stationary. For the statistically steady state, the eigenvectors of B_∞ are ordered according to their contribution to the variance and are called "stochastic optimals" (Farrell and Ioannou, 1996) for the linearized dynamics (24). The leading stochastic optimal (shown as *sol* in figure 7), most effectively excites the stationary variance. The stochastic optimals are different to the eigenvec-

tors which span the maintained variance (EOFs). The leading EOF is the first eigenvector of the covariance matrix $(E\{x_i x_j\})_{i,j=1,2}$ and interestingly, the first EOF coincides almost with the most unstable mode. The leading stochastic optimal, however, points almost into the direction of the most efficient excitation vector e_1^* (figure 7).

The long-term variance in an ensemble of trajectories is maximal, when the permanent forcing is large for high latitude salinity. The different realizations of $x(t)$ for (25) are due to the random weather fluctuations. Our stochastic optimal vector suggests that the long-term predictability of the THC can be therefore mainly limited by the knowledge of higher frequency atmospheric fluctuations in the high latitude fresh water flux. The effective span of the variance, the first EOF, is much different from the vector which most effectively excites the stationary variance - a common feature of non-normal systems (Farrell and Ioannou, 1996).

It is useful to calculate the ensemble response variance $\Xi(\omega)$ which is given by the Fourier transform of the variance

$$Var(x) = \frac{1}{2\pi} \int_{\mathsf{R}} \Xi(\omega)\, d\omega \quad . \tag{27}$$

The ensemble response variance $\Xi(\omega)$, has a complicated polynomial structure and is shown in figure 8 (solid line). In order to make x and Ξ dimensionless, salinity and temperature are scaled here by the haline and thermal expansion coefficients. This figure shows that the long-term stochastic response greatly exceeds the function $\Xi_{orth}(\omega)$ (dashed line). This function is obtained by the summation of the contributions from the poles of the resolvent, as is would be appropriate for a system with two orthogonal eigenmodes with eigenvalues λ_1 and λ_2:

$$\Xi(\omega) \geq \Xi_{orth}(\omega) = \frac{1}{\omega^2 + \lambda_1^2} + \frac{1}{\omega^2 + \lambda_2^2} \quad . \tag{28}$$

The equality holds only for normal matrixes A (Farrell and Ioannou, 1996).[2]

3.5 Remarks

Several studies analyzed the THC's long-term variance using stochastic upper boundary conditions. Mikolajewicz and Maier-Reimer (1990) used an

[2]In the mathematical literature, the greatly enhanced frequency response for non-normal operators is considered in the framework of pseudospectral analysis (e.g. Trefethen et al., 1993; Reddy, 1993).

ocean general circulation model (OGCM) under mixed boundary conditions with superimposed white noise forcing in the fresh water flux. They found a strong secular mode of variability with a period of approximately 320 years. Other studies using models with different levels of complexity (as e.g. Cessi, 1994; Weisse et al., 1994; Griffies and Tzipermann, 1995) find also that the long-term variability is greatly enhanced when noise is added. In terms of our terminology, their models are forced by perturbations that are close to our leading stochastic optimals for the long-term variability. However, the mechanisms responsible for the variability in more complex models is different to those simulated in stochastical box models. We come to this point in section 5 considering a coupled ocean circulation-energy balance model.

Our study shows that a proper conceptual model of the THC's variability and predictability can never be one-dimensional since two different regimes exists. In one-dimensional models (as that suggested by Griffies and Bryan, 1997 b), the stochastic optimal, the optimal excitation vector and the most unstable normal mode coincide with each other. Furthermore, the modes interact such that the ensemble response variance is larger than the summation of two different autoregressive processes for the distinct time-regimes. This seems to be important since two different time regimes for $t > 10$ and < 10 years have been seen in the spectrum of the GFDL (Delworth et al., 1994; Griffies and Bryan, 1997 b) and a MPI (Timmermann et al., 1997) coupled models. It is conceivable that fluctuations in salinity explain most of the interdecadal climate variability in these models.

Farrell and Ioannou's (1996) concept and our analysis show the strong influence of non-normal operators on stability properties, which seems to be a quite general feature of fluid dynamical systems (Reddy, 1993; Trefethen et al., 1993).[3] The methods presented here will be applied to other hydrodynamic instability problems, such as baroclinic instability (Farrell and Ioannou, 1996).

We find that the information loss of the trajectory is due to the dominant

[3]Many instability analyses in fluid dynamics, based on normal mode theory, have been revised after recognizing that a transient amplification can wrongly estimate the stability and bifurcation (for a discussion see: Trefethen et al., 1993; Farrell and Ioannou, 1996).

singular vector, associated with an amplification factor σ_1:

$$\max_{||x(0)||\neq 0} \left(\frac{|| x(t) ||}{|| x(0) ||} \right) = \sigma_1 \quad . \tag{29}$$

We want to know which processes in the coupled atmosphere-ocean system may restrict the predictability. The definition of the singular vector with amplification σ_1 demands that an instability mechanism must be responsible for the error growth. For our model, the basic instability mechanism is due to high latitude salinity. We shall discuss this point in light of previous predictability studies.

Nese and Dutton (1993) couple a low order atmospheric model based on the Lorenz (1965)-model to an ocean shallow layer model with uniform depth and no salinity effects. They found that the atmospheric predictability regimes are more persistent in the presence of the ocean model due to the strong thermal coupling which act as a stabilizing mechanisms for the Lorenz (1965)-regimes. The dominant singular vector or the local divergence rate is reduced due the presence of the underlying ocean component.

In our model, the basic instability mechanism is not due to the atmosphere. The atmospheric model component removes temperature gradient anomalies, providing for a climatological mean meridional temperature gradient. The baroclinic instability mechanism, which sets the timescale for the transitions between the weather regimes (Nese and Dutton, 1993; Palmer, 1996), is responsible for a poleward heat transport due to highs and lows in a statistical sense. This effect is modeled by diffusion which makes the SST therefore highly predictable, because the inherent atmospheric variability/unpredictability is averaged out.

Griffies and Bryan (1997 b) investigated the predictability of temperature and salinity anomalies in the North Atlantic using a coupled GCM. They found that surface temperature is predictable for a few years only. After this time, the information in the ensemble is of no more use than the information already contained in the climatologic record. In their coupled GCM, salinity, dynamic topography, and subsurface quantities are much more predictable than SST. The predictability seems to be limited by the overlying chaotic atmospheric variability. Additionally, their system is hardly predictable in regions of active convection where the ocean shows an internal variability due

to the convective adjustment scheme. Their ensembles diverge for different realizations of the synoptic scale weather, whereas salinity and subsurface quantities are much more persistent. In particular, the THC is relatively well predictable in their ensemble experiments.

In contrast, our box model is designed to capture some basic features of the *climatological mean state*. In contrast to sea surface temperature, there is no fast removing mechanism for sea surface salinity anomalies and initial errors can be amplified. It is likely that SST is predictable in the climate mode, defined by an ensemble average over synoptic realizations. When neglecting sea ice effects, SST is the only quantity which couples to the atmosphere. Since there are indications for coupled modes in coupled GCMs (see e.g. Timmermann et al., 1997) on interdecadal time scale, SSTs should be predictable on this time scale leading to climate modes of variability. Coupled atmosphere-ocean modes require therefore a negative (stabilizing) feedback mechanism to observe these modes.

4 Sensitivity to different climate conditions

Here, we want to explore the sensitivity of NADW formation to the mean climate. Our "coarse" box model may be useful to investigate the sensitivity of the ocean circulation to salinity perturbations under different mean climatic conditions. Little is known about the circulations during paleoclimatic states in which large freshenings have occured because of the sparse data and the data uncertainties. Furthermore, coupled circulation models need artificial fluxes (flux corrections) to overcome model deficiencies and to simulate correctly the current climate. Locally, these flux corrections can be very large (see Gates et al. (1993) for some coupled GCMs). When simulating other climate states the flux correction technique is not apropiate, because the correction fluxes are tuned for the present climate state.

In our nonlinear model, the sensitivity of the THC depends on the chosen basic state of the model $(\Delta S^\circ, \Delta T^\circ)$. If the heat and fresh water boundary fluxes are fixed (corresponding to $\epsilon = 1$ and $K_2 = 0$), the critical perturbation S_{crit} in equation (16) reduces to

$$S_{crit} = 2\left(-\Delta S^\circ + \frac{\alpha}{\beta}\Delta T^\circ\right) \tag{30}$$

which is always negative for $\Phi = c\beta\Delta S^0 - c\alpha\Delta T^0 > 0$ considered here. In this case the circulation is globally stable with respect to perturbations. For a system with small thermal feedback and no anomalous fresh water flux ($K_2 = 0$ and $\epsilon < 0.5$), the critical perturbation is approximately

$$S_{crit} \approx 2\left(-\Delta S^\circ + \frac{\alpha}{2\beta}\Delta T^\circ\right) \quad . \tag{31}$$

Such systems are more sensitive than systems with fixed boundary fluxes with S_{crit} in (30). We find that climate states with a strong thermally dominated deep water formation (large $\mid \Delta T^\circ \mid$ and small salinity differences $\mid \Delta S^0 \mid$) favor the stability of the THC expressed by large values of critical salinity perturbation S_{crit}. The dashed line in figure 9 shows the critical salinity perturbation in the coupled case. The slopes of the curves ly between the case (30) with slope $\beta/\alpha\,(= 5.3$ K/psu) and case (31) with slope $2\beta/\alpha$.

With a changed background temperature, the thermal expansion coefficient α will change. In order to include this effect, a simplified nonlinearity in the

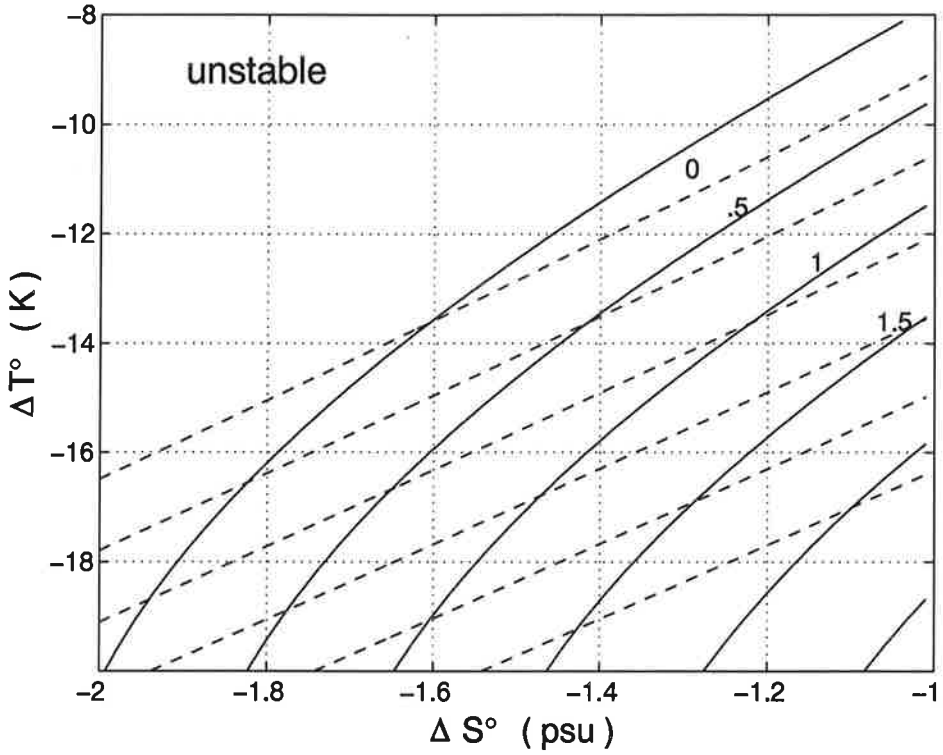

Figure 9: Critical salinity perturbation S_{crit} for the coupled system in the parameter space $(\Delta T^0, \Delta S^0)$ with contour interval 0.5 psu. The dashed lines are for fixed thermal expansion coefficient α, whereas for the solid lines a changed thermal expansion coefficient α is assumed. The coupled system is linearly unstable above the curve $S_{crit} = 0$. These climate states cannot be realized in nature.

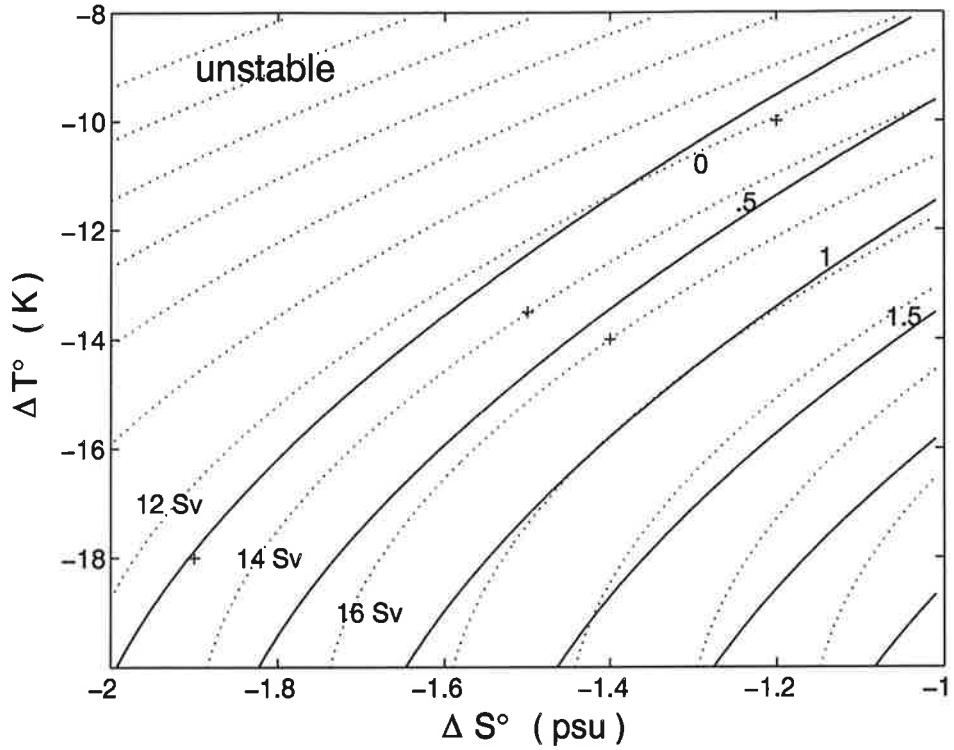

Figure 10: Same as figure 9 for the solid lines. The overturning rates Φ° are plotted as dotted lines with contour interval 2 Sv. The crosses (+) in the figure correspond to the different climatic states in table 1.

equation of state as in Zhang et al. (1993) is assumed:

$$\rho(T,S) = 1003.0 + 0.77\,S - 0.072\,T \quad (1 + 0.072\,T) \quad . \qquad (32)$$

This modification in the model is done such that the density for today's climate (tuned in Lohmann et al., 1996) is equal for the linear and nonlinear equation of state. Furthermore, the temperature dependent components K_2 and K in the model are included, which can be justified by the Clausius-Clapeyron equation (Lohmann et al., 1996 b). The resulting critical salinity perturbations S_{crit} (figure 9, solid line) show a destabilizing effect for cold temperatures and stabilizing effect for warm temperatures. The differences between the solid and dashed lines are mainly due to the nonlinearity in the equation of state (32), whereas the other nonlinear effects of K_2 and K are much weaker. Freshenings in colder climates are therefore more effective in perturbing the THC than in warm climates. The colder the temperature, the weaker is the effect of temperature variations on density. For cold climate states, the meridional overturning rates are reduced due to the changed thermal expansion coefficient.

Climate	$-\Delta S^0$ psu	$-\Delta T^0$ K	Φ^0 Sv	α 1/K	S_{crit} psu
a)	1.4	14	16	0.147	0.62
b)	1.5	13.5	14	0.150	0.25
c)	1.2	10	12	0.168	0.12
d)	1.9	18	13	0.127	0.06

Table 1: Table for critical salinity perturbations for different climates which can also be obtained from figure 10. The dynamics for climates a)-c) are shown in the thermo-haline phase space (figure 3).

Figure 10 indicates that the THC with North Atlantic Deep Water formation is possible only in a specific parameter regime for temperature and salinity and that the critical perturbation S_{crit} is mainly determined by Φ°, the strength of the background meridional mass transport. Basic states with small overturning are not stable and therefore not realized in nature. In the box model, we find a critical transport of about 12 Sv. Four different climate states are shown additionally, which are denoted as climates a)-d) in table 1. The climate states are ordered according to the critical salinity perturbation S_{crit}. Climate c) corresponds to a warmer climate, whereas climate d) corresponds to a glacial climate with stronger temperature and salinity contrasts. The estimated perturbation associated with the recent Great Salinity Anomaly (Dickson et al., 1988) was of the order of $S_{GSA} = 0.048$ psu for the high latitude box. The critical perturbation for climate d) is therefore within the range of the natural salinity fluctuations. For the climate states a)-c), the thermo-haline phase space trajectories (figure 3) reveal that these climate states have a slightly different long-term evolution because the eigenmode e_1 depends on α/β. The short-term response, corresponding to vector e_2, is very similar for all climate states. The non-normality of the eigenvectors increases with colder climate due to eigenmode e_1. The angle between the eigenvectors e_1 and e_2 decreases in a colder climate, which increases the transient growth of temperature necessary to compensate the density reduction by salinity.

The long-term variance (26) in our coupled system is larger, relative to the case of a normal matrix A. Let Θ denote the angle between the eigenmodes e_1 and e_2. Farrell and Ioannou (1996) show that the increase in variance

due to the non-normality is proportional to the square of the cotangens of Θ, vanishing for $\Theta = \pi/2$. This means that the long-term variance increases for colder climate states with smaller angle Θ (figure 3), which might explain a stronger THC variability in the past.

The large sensitivity for cold climates relative to warm climate is consistent with studies using models with different levels of complexity. Manabe and Bryan (1985) found that the THC is very sensitive to a reduction of 50% in the atmospheric CO_2 content and relatively insensitive to a doubled CO_2 content. In the reduction case, the poleward mass transport is reduced and the surface density in high northern latitudes decreases as a net-effect. In more recent experiments (Manabe and Stouffer, 1994), they find that after initial weakening, the equilibrium strength of the THC hardly changes with increased CO_2, because the increase in the meridional density gradient due to the general increase in temperature compensates the reduction of the density gradient due to the reduction of high latitude salinity. Recent coupled GCM experiments (Tzipermann, 1997) are consistent with our results that the strength of the THC determines the sensitivity of the THC to salinity fluctuations. Tzipermann (1997) finds a much greater climate instability for a wide range of weak mean states of the THC.

A stabilizing temperature feedback for the THC (Rahmstorf and Willebrand, 1995) is due to a weakened overturning: Lower sea surface temperatures increase the density at high latitudes. The temperature feedback is weaker for colder climates than for warmer climates due to the nonlinearity in the equation of state. The changed temperature feedback has also been found by Winton (1997) and Prange et al. (1997). Prange et al. (1997) consider the advective feedback in a coupled box model for a warmer and colder climate state, whereas Winton (1997) using a two dimensional ocean model finds that convection is affected by the weakened temperature feedback in a cold climate. It could be that glacial climate states are more unstable than interglacial states due to the changed salinity effect on density. However, we would like to emphasize that our mechanism for the relatively high sensitivity of cold climate states could be one effect among several others in the climate system, e.g. sea ice effects or changed high latitude vertical mixing.

5 Experiments with a coupled ocean circulation-energy balance model

The feedbacks involved in an ocean circulation model coupled to a moist energy balance model of the atmosphere are analyzed and compared to those from our box model.

5.1 Model

The ocean model used is the 1991-version of the GFDL primitive equation model MOM (Pacanowski et al., 1993, 1991) which is based on the work of Bryan (1969) and Cox (1984). The ocean model has a resolution of two degrees in the horizontal and 16 vertical levels. The geometry of the ocean model is a 64^0 wide sector with flat bottom topography (5700 m deep) ranging from the equator to 70^0 N. Different time steps for tracer (12 h) and velocity (1 h) are used. The model is forced by zonally averaged wind stress computed from the data set of Hellerman and Rosenstein (1983).

The atmosphere model is a moist energy balance model (EBM), similar to that described earlier (Lohmann et al., 1996 a; Lohmann and Gerdes, 1996). The atmospheric transport processes by transient eddies are modeled by diffusion.[4] The only difference to earlier versions of the model is that it is regionalized over the Atlantic basin: The atmosphere has almost identical geometry and river catchment area as the analytical box model. The resolution of the atmospheric model is 10^0 in latitudinal direction. We have chosen this resolution, because the atmospheric heat transport by baroclinic eddies can be parameterized on scales o(1000 km) by diffusion (Green, 1970; Lorenz, 1979) transporting in a statistical sense heat and moisture poleward. With this resolution, we can avoid the unphysical interaction of the oceanic convection scheme (Cessi, 1996) and atmospheric diffusion on scales corresponding to the oceanic grid.[5]

[4] The EBM is available under anonymous ftp at ftp.dkrz.de /pub/Outgoing/gerrit/EBM

[5] The diffusive parameterization is not justified physically on the finer oceanic grid, and therefore, convection and diffusion should be modeled on different spatial scales.

5.2 Experimental setup

The ocean was spun up under restoring boundary conditions for temperature using simplified bulk formulas (as in Lohmann and Gerdes, 1996). The fresh water flux field is obtained by multiplying the zonal mean fresh water fluxes of Sellers (1969) by three. Comparing the zonally averaged fresh water fluxes of Sellers (1969) and the fluxes diagnosed an ocean model integrated under restoring condition for salinity, Lohmann et al. (1996 a, figure 3) found that a factor of about three seems to be adequate for the North Atlantic. This is due to the enhanced hydrological cycle over the Atlantic compared to the zonal mean.

The integration is then continued in a coupled mode until a steady state is reached. The resulting mean meridional salinity gradient is about -1.3 psu, and the maximal overturning rate is 27.4 Sv. The overturning stream function of the reference state is shown in the upper panel of figure 11. Deep water is formed north of 60° N, and upwelling is found elsewhere.

5.3 Sensitivity

In the coupled ocean circulation-energy balance model (OGCM-EBM), we analyze the response of NADW formation with respect to a perturbation in sea surface salinity and compare the results with those of our box model. A large salinity perturbation of -1.5 psu is introduced in the region $60^0 - 70^0$ N. The amount of deep water formation is strongly reduced in response to this perturbation (figure 12). The coupled system recovers after about 100 years and reaches the initial state.

The lower panel in figure 11 shows the overturning stream function when the THC is at its minimum. The deep water formation is interrupted, and a strong halocline exists in the northern North Atlantic (not shown), inhibiting convection. This mechanism responsible for the high sensitivity of the THC was originally found by Bryan (1986) using a sector ocean model. Because the halocline suppresses NADW formation, the mechanism is called "polar halocline catastrophe".

In our coupled OGCM-EBM, the vertical heat transfer is reduced in the ocean, cooling the mixed layer and air temperatures. When the THC is min-

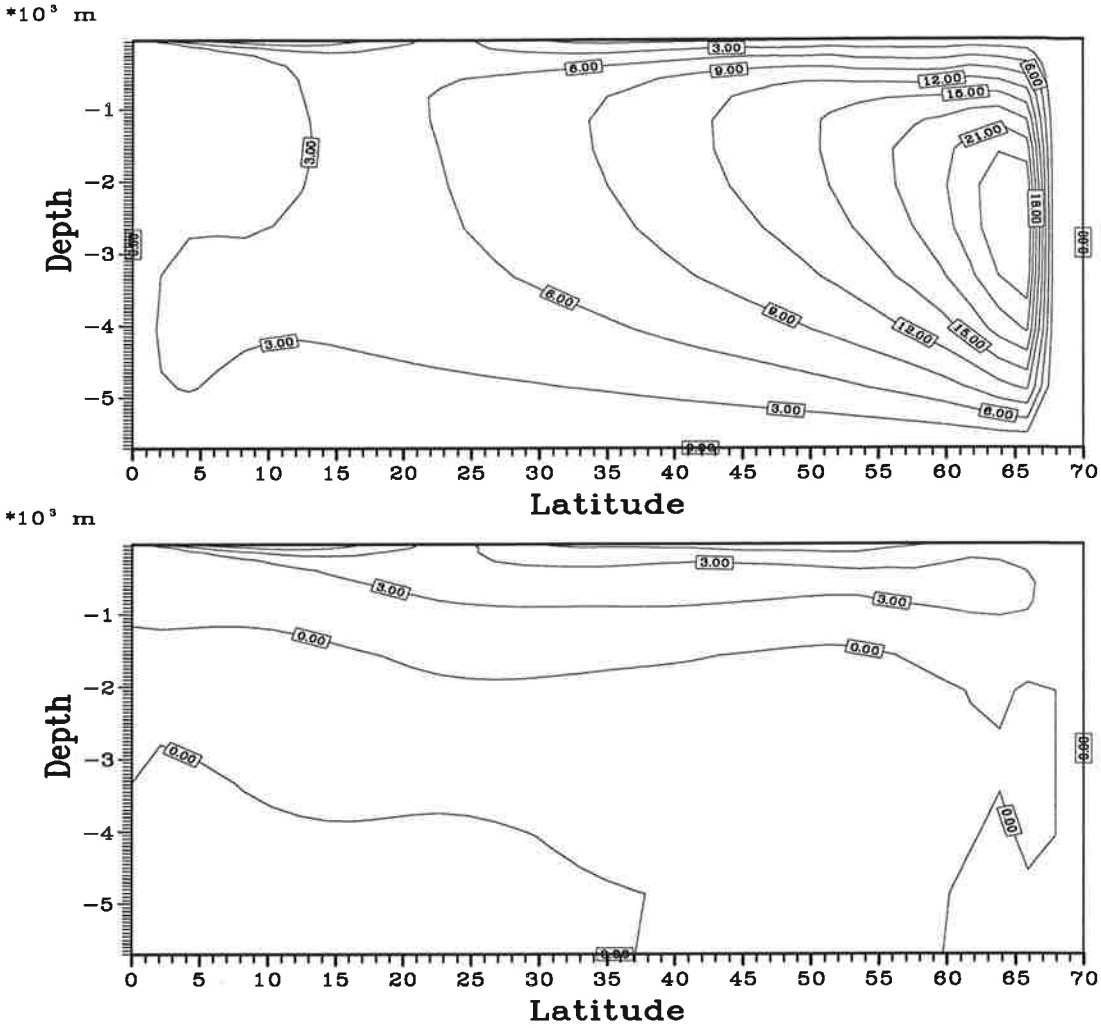

Figure 11: Stream function for the zonally integrated transport in Sv ($10^6\, m^3 s^{-1}$) for the North Atlantic. The upper panel shows the reference case with a maximal overturning rate of 27.4 Sv. The lower panel shows the circulation, 4 years after the perturbation in high latitude salinity, when the circulation has its minimal overturning. The contour interval is 3 Sv.

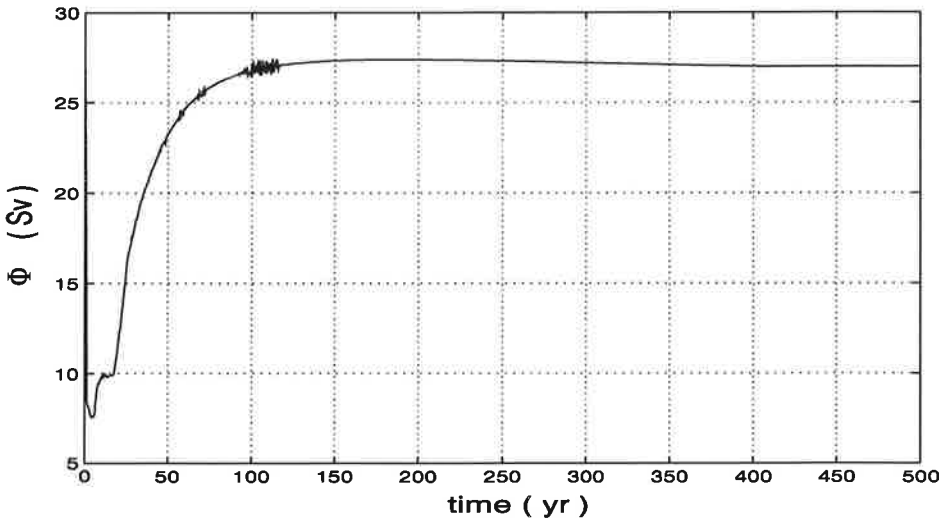

Figure 12: Time series of the maximal zonally integrated mass transport in the northern hemisphere after a perturbation in sea surface salinity. The circulation recovers completely after few hundred years.

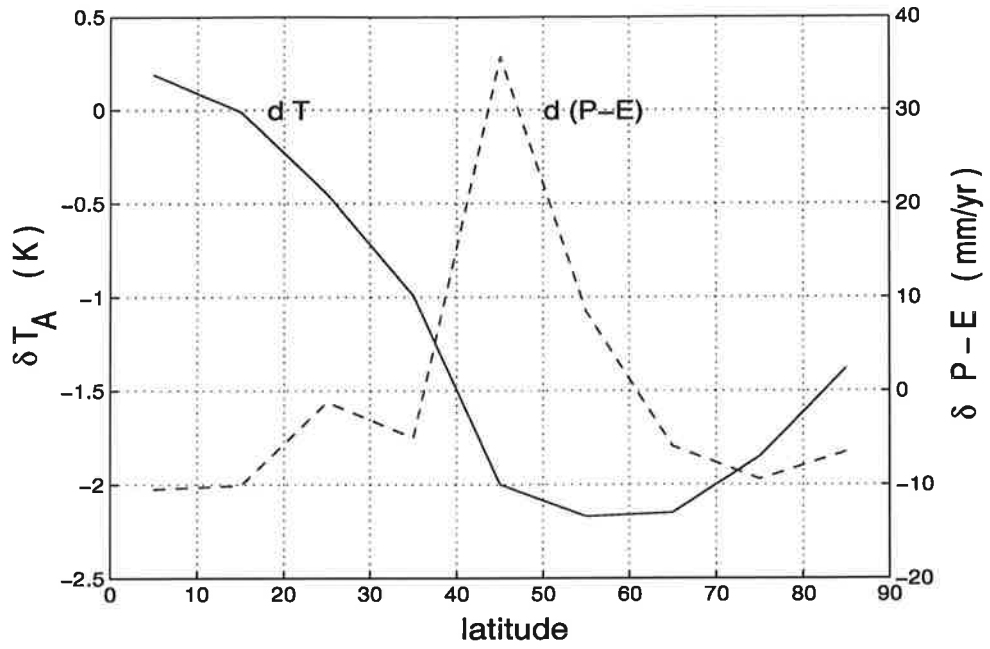

Figure 13: Change of atmospheric surface temperature and fresh water flux, 4 years after a salinity perturbation of -1.5 psu between 60° and 70°. The high latitude temperature is decreased (solid line). The hydrological cycle is increased resulting in positive $\delta(P-E)$ values for $40° - 60°$ (dashed line).

imal, the heat flux at the ocean-atmosphere interface is reduced, decreasing the mixed layer depth due to less vertical mixing. SST and air temperature at high latitudes are lowered by about 2 K (figure 13), whereas the low latitude temperature is nearly unchanged.

The strong cooling increases the sea surface density at high latitudes, compensating for the large fresh water input. However, the compensation due to the temperature effect is not strong enough to overcome the effects of the high latitude halocline which suppresses deep convection (figure 11, lower panel). During the recovery towards the initial equilibrium state, the cold temperatures enhance convection, mixing saline and warm subsurface water to the surface. After a few hundred years, the circulation has recovered completely.

The increased meridional temperature gradient ($\partial_y T_A$) developing in response to the salinity perturbation favors baroclinic eddy activity increasing the atmospheric northward heat transport (figure 14). The strength of the hydrological cycle increases too, and more atmospheric water vapour is transported poleward. Positive fresh water flux anomalies are simulated in

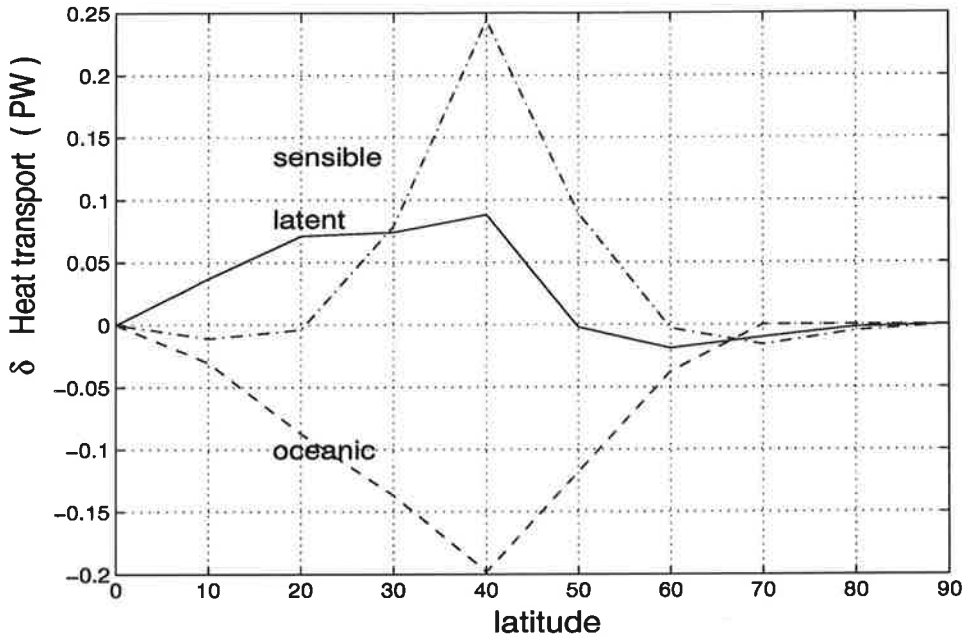

Figure 14: Change of northward heat transport in the coupled atmosphere-ocean model, 4 years after the high latitude salinity perturbation. The oceanic heat transport is reduced while the atmospheric sensible and latent heat transports are enhanced.

the region $40° - 60°$ N (figure 13, dashed line) whereas $\delta(P - E)$ is negative elsewhere. Thus, the hydrological destabilizes the water column in the region north of 60° N.

In figure 14, the heat transport contributions are shown as simulated 4 years after the high latitude salinity perturbation was introduced. The oceanic northward heat transport is reduced by about 40% of its initial value. The cooling due to the reduced oceanic heat transport is partly compensated by the atmospheric sensible and latent heat transports. A similar feature has also been observed in coupled circulation models in which the atmospheric dynamics are explicitly resolved (Schiller et al., 1996). The increased atmospheric heat transport warms the air in mid-latitudes, which has a a destabilizing effect on the THC.

5.4 Discussion

We have shown in the sensitivity experiment with the coupled OGCM-EBM that a negative salinity anomaly at high latitudes causes a reduction in deep water formation which is consistent with observational data from sediment cores (Mc Cave et al., 1995). The coupled model's response shows a reduced

oceanic heat and enhanced atmospheric heat and moisture transports, when the deep water formation is suppressed.

It is useful to compare the results obtained from the box model and the OGCM-EBM. Recently, it has been shown that Stommel's (1961) box model dynamics can be retrieved from dynamical equations when neglecting rotational effects (Maas, 1994; van der Schrier and Maas, 1997). Furthermore, some ocean circulation studies (Hughes and Weaver, 1994; Rahmstorf, 1996; Griffies and Bryan, 1997 b) find a close correlation between the meridional density gradient and meridional mass transport. We hope therefore that the box model dynamics captures some basic features of ocean circulation models.

From figure 13, we roughly estimate K_2 for the oceanic basin north of 40° N to be approximately 8 $mm\,yr^{-1}\,K^{-1}$. Note the spatial structure of $\delta(P-E)$ when the THC is in its minimum. Highly idealized box models, such as e.g. Nakamura et al. (1994) and ours, overestimate the destabilizing effect of the poleward water vapour transport. We find that the feedback on salinity is more localized than that for temperature. However, the fresh water balance of the North Atlantic is still an open question, whether the high latitude salinity is affected by the oceanic conveyor itself or by the latent heat transport. It is conceivable that both the oceanic salt transport into the Atlantic basin (Rahmstorf, 1996) and the change of the atmospheric latent heat transport affect sensitively the upper oceanic salt transport into NADW formation areas. We address this question to a further study, where the Atlantic's equilibrium fresh water balance (as in Zaucker and Broecker, 1992) will be analyzed for different climatic states.

The heat flux parameterization in the OGCM-EBM is scale dependent (as proposed by Rahmstorf and Willebrand, 1995) due to the diffusive transient eddy term part of the EBM. Therefore, the thermal response in the OGCM-EBM cannot be tuned in a system using mixed boundary conditions by changing the thermal adjustment Q_2 locally. This could be done in the box model, because the transport term is only due to the single parameter K in the atmospheric model. With our temperature anomaly of -2 K (figure 13) and a change in atmospheric heat transport of 0.35 PW (figure 14), we estimate the coefficient K to be of the order of $10\,Wm^{-2}K^{-1}$ which is

consistent with the box model estimate.

Different mechanisms in the OGCM-EBM and box model may be responsible for the weakening of the THC. In the OGCM-EBM, a convective instability mechanism triggers the advective instability (Lenderink and Haarsma, 1994; Rahmstorf, 1995). The convective instability mechanism is not included in the box model, but we find that both instability mechanisms work in the same direction: A weakened overturning lead to colder air and colder high latitude SST's. This destabilizes the water column enhancing convection (convective feedback) and leading to enhanced meridional transport (advective feedback) stabilizing the THC.

6 Summary and Conclusions

We have presented an analytical solution for the Stommel (1961)-type box models. Starting from the analytical solution of Stommel's model, we found a class of exact solvable nonlinear differential equations. The method to obtain the solution will be described in a corresponding mathematical paper (Schneider and Lohmann, 1997).

Using the analytical solution of a coupled atmosphere-ocean version of Stommel's (1961) box model, the sensitivity of North Atlantic Deep Water formation has been analyzed with respect to the atmospheric transport and the mean basic state. We show that the representation of the atmospheric model component does strongly determine the critical salinity perturbation for which the linearly stable system breaks down.

The more complex OGCM-EBM shows a qualitative agreement with the box model's response, although different mechanisms are responsible for the weakening of the THC. In both types of models, we found that the temperature response is very fast compared to that of the most unstable modes, which is due to a mixed temperature/salinity vector. This is consistent with the rapid cooling associated with the time after the Younger Dryas event (Dansgaard et al., 1993). We found that the box model overestimates the destabilizing effect of the eddy moisture transport due to the coarse box model's resolution. The fresh water balance of the North Atlantic is still an open question. This is subject of a further investigation using a coupled GCM, analyzing fresh water transports for the present, a colder, and a warmer climatic state, respectively.

In our simple coupled box model, haline perturbations in the northern North Atlantic provide most effective excitations for the thermohaline circulation. In the phase space, the optimal perturbation as an initial value problem is perpendicular to the temperature eigenmode of the system and has little resemblance with the most unstable mode and the leading EOF. This feature is independent on the climatic background state. The THC's dynamics in our box model is affected by the non-orthogonality of its eigenvectors and we revealed that the simplest conceptual model for the THC's variability must be at least two-dimensional in phase space. Two distinct time regimes can

be furthermore identified.

We address the question whether the climate predictability can be captured by a simple low order model. The dominant error growth vector is closely related to the salinity anomalies in the phase space of the box model. High latitude haline anomalies are responsible for the short-term amplification of the forecast ellipsoid, because haline perturbations provide for a instability mechanism in the model. The climatological sea surface temperature is much more predictable than sea surface salinity, because the atmospheric damping is strong for temperature and weak for salinity. Our result differs from that of Griffies and Bryan (1997 a, b) who use a coupled GCM. Their predictability seems to be limited by the overlying chaotic atmospheric variability. Using a model with much more degrees of freedom and other instability mechanisms, their ensemble experiments show that sea surface temperature is predictable for a few years only and the ensemble is of no more use than the information already contained in the climatologic record. Our box model, however, deals with the predictability of the climatological mean state and captures therefore a different feature of the coupled atmosphere-ocean system. Our analysis suggests that the predictability limit is largely associated with the model's instabilities. More studies using models with different levels of complexity are required to get more insight into the mechanisms of decadal climate predictability.

Considering the long-term variability in the North Atlantic, the atmospheric noise is integrated by the THC. The leading EOF, a mixed temperature/salinity vector, is optimally excited by salinity fluctuations in the northern North Atlantic induced by the weather noise. With our low order model, we can show that fresh water flux fluctuations play thus an important role influencing the thermohaline circulation and long-term variability. In a future study, we shall test our hypothesis that long-term fluctuations of the THC are associated with fluctuations in high latitude sea surface salinity with a coupled GCM.

The analytical box model reveals that the sensitivity is stronger for colder than for warmer climate conditions because density is more affected by salinity for lower temperatures. This effect may be important in order to understand paleoclimatic climate shifts associated with large freshenings (e.g.

Boyle and Keigwin, 1987; Sarnthein et al., 1994). Our results suggest that the strength of the NADW circulation determines the sensitivity of the THC to salinity fluctuations. This is also supported by the recent coupled GCM experiments of Tzipermann (1997) who find inherently unstable climate behavior due to weak THC. Beside several other effects, it may well be that the different sensitivities of the THCs in the GFDL (Manabe and Stouffer, 1995, 1996) and a MPI (Schiller et al., 1996) coupled GCM are partly due to the different overturning rates in the reference climates.

We think that our nonlinear systems presented here are good prototype models to understand climate variations related to salinity perturbations, and we hope that our low-order box model is a helpful tool to understand the long-term variability and predictability of the THC in more complex models.

Acknowledgements

M. Latif, A. Timmermann, R. Gerdes, C. Eckert, and E. Maier-Reimer are gratefully acknowledged for their improvements to the manuscript. A part of the presented work was inspired by a course "Decadal climate variability-Dynamics and predictability" at the MPI. We thank Prof. Dr. K. Hasselmann and Prof. Dr. W. Maaß for their support.

References

[1] Blumenthal, B., 1991: Predictability of a coupled ocean-atmosphere model. J. Climate 4,766-784.

[2] Bond, G.C., Heinrich, H., Broecker, W., Labeyrie, L., McManus, J., Andrews, J., Huon, S., Jantschik, R., Clasen, S., Simet, C., Tedesco, K., Klas, M., Bonani, G., and Ivy, S., 1992: Evidence for massive discharges of icebergs into the North Atlantic ocean during the last glacial period. Nature 360,245-249.

[3] Boyle, E.A., and Keigwin, L.D., 1987: North Atlantic thermohaline circulation during the past 20,000 years linked to high latitude surface temperature. Nature, 330,35-40.

[4] Broecker, W.S., Peteet, D.U., and Rind, D., 1985: Does the ocean-atmosphere system have more than one stable mode of operation. Nature 315,21-26.

[5] Bryan, F., 1986: High latitude salinity effects and inter hemispheric thermohaline circulations. Nature 323,301-304.

[6] Bryan, K., 1969: A numerical method for the study of the circulation of the world ocean. J. Comput. Phys. 4,347-376. J. Phys. Oceanogr. 25,1998-2010.

[7] Cessi, P., 1994: Simple box model of stochastically forced thermohaline force. J. Phys. Oceanogr. 24,1911-1920.

[8] Cessi, P., 1996: Grid-scale instability of convective-adjustment schemes. J. Marine Res. 54,407-420.

[9] Chen, D., Gerdes, R., and Lohmann, G., 1995: A 1-D atmospheric energy balance model developed for ocean modelling. Theor. Appl. Climatol. 51,25-38.

[10] Cox, M.D., 1984: A primitive equation,3-dimensional model of the ocean. GFDL Techn. Report 1, Princeton University.

[11] Dansgaard, W., Johnsen, S.J., Causen, H.B., Dahl-Jensen, D., Gundestrup, N.S., Hammer, C.U., Huidber, C.S., Steffensen, J.P., Sveinbjornsdottir, A.E., Jouzel, J., and Bond, G., 1993: Evidence for general instability of past climate from a 250-kyr ice-core record. Nature 364,218-220.

[12] Dickson, R.R., Meincke, J., Malmberg, S.A., and Lee, A.J., 1988: The "Great Salinity Anomaly" in the northern Atlantic 1968-1982. Prog. Ocean. 20,103-151.

[13] Eckert, C., and Latif, M., 1997: Predictability of a stochastically forced hybrid coupled model of El Niño. J. Climate (in press).

[14] Fairbanks, R.G., 1989: A 17,000 year glacio-eustatic sea level record: Influence of glacial melting rates on the Younger Dryas event and deep ocean circulation. Nature 342,637-642.

[15] Farrell, B.F., and Ioannou, P.J., 1996: Generalized stability theory. Part I: Autonomous operators. J. Atm. Sci. 53,2025-2040.

[16] Gates, W.L., Cubasch, U., Meehl, G.A., Mitchell, J.F.B., Stouffer, R.J., 1993: An Intercomparison of selected features of the control climates by coupled ocean-atmosphere general circulation models. Genf WMO WCRP.

[17] Goswami, B.N., and Shukla, J., 1991: Predictability of a coupled ocean-atmosphere model. J. Climate 4,3-22.

[18] Green, J.S.A., 1970: Transport properties of large-scale eddies and the general circulation of the atmosphere. Q. J. Roy. Meteor. Soc. 96,157-185.

[19] Griffies, S.M., and Tzipermann, E., 1995: A linear thermohaline oscillator driven by stochastic atmospheric forcing. J. Climate 8,2440-2453.

[20] Griffies, S.M., and Bryan, K., 1997 a: Predictability of North Atlantic Multidecadal Climate Variability. Science 275,181-184.

[21] Griffies, S.M., and Bryan, K., 1997 b: A Predictability Study of Simulated North Atlantic Multidecadal Variability. Climate Dynamics (in press).

[22] Hasselmann, K., 1976: Stochastic climate models, Part 1, Theory. Tellus 28,289-485.

[23] Hellerman, S, and M. Rosenstein, 1983: Normal monthly wind stress over the world ocean with error estimates. J. Phys. Oceanogr. 13,1093-1104.

[24] Hughes, T.M.C., and Weaver, A.J., 1994: Multiple equilibria of an asymmetric two-basin model. J. Phys. Oceanogr. 24,619-637.

[25] Keigwin, L.D., Jones, G.A., Lehmann, S.J., and Boyle, E.A., 1991. Deglacial meltwater discharge, North Atlantic deep circulation, and abrupt climate change. J. Geophys. Res. 96,16811-16826.

[26] Latif, M. and Barnett, T.P., 1994: Causes of Decadal Climate Variability over the North Pacific and North America. Science 266,634-637.

[27] Lazier, J.R.N., 1988: Temperature and salinity changes in the deep Labrador Sea, 1962-1986. Deep Sea Res. 35,1247-1253.

[28] Lehmann, S.J., and Keigwin, L.D.,1982: Sudden changes in North Atlantic circulation during the last deglaciation. Nature 356,757-762.

[29] Lenderink, G., and Haarsma, R.J., 1994: Variability and multiple equilibria of the thermohaline circulation associated with deep-water formation. J. Phys. Oceanogr. 24,1480-1493.

[30] Lohmann, G., and Gerdes, R., 1996: Sea ice effects on the sensitivity of the thermohaline circulation. J. Climate (submitted).

[31] Lohmann, G., Gerdes, R., and Chen, D., 1996 a: Sensitivity of the thermohaline circulation in coupled oceanic GCM-atmospheric EBM experiments. Climate Dynamics 12,403-416.

[32] Lohmann, G., Gerdes, R., and Chen, D., 1996 b: Stability of the thermohaline circulation in a simple coupled model. Tellus 48 A,465-476.

[33] Lorenz, E.N., 1965: A study of the predictability of a 28-variable atmospheric model. Tellus 7,157-167.

[34] Lorenz, E.N., 1979: Forced and free variations of weather and climate. J. Atm. Sci. 36,1367-1376.

[35] Maas, L.R.M., 1994: A simple model for the three-dimensional thermally and wind-driven ocean circulation. Tellus 46 A,671-680.

[36] Manabe, S. and K. Bryan, 1985: CO_2-induced change in a coupled ocean-atmosphere model and its paleoclimatic implications. J. Geophys. Res. 90,11689-11707.

[37] Manabe, S., and Stouffer, R.J., 1994: Multiple-century response of a coupled ocean-atmosphere model to an increase of the atmospheric carbon dioxide. J. Climate 7,5-23.

[38] Manabe, S., and Stouffer, R.J., 1995: Simulating of abrupt climate change induced by freshwater input into the North Atlantic Ocean. Nature 378,165-167.

[39] Manabe, S., and Stouffer, R.J., 1996: Simulation of Younger Dryas-like phenomenon by a coupled ocean-atmosphere model. Paleoceanogr. (in press).

[40] Marotzke, J. and Stone, P.H., 1995: Atmospheric transports, the thermohaline circulation, and flux adjustments in a simple coupled model. J. Phys. Oceanogr. 25,1350-1364.

[41] McCave, N., Manighetti, B., and Beveridge, N.A.S., 1995: Circulation in the glacial North Atlantic inferred from grain-size measurements. Nature 374,149-151.

[42] Mikolajewicz, U., Maier-Reimer, E., 1990: Internal secular variability in an ocean general circulation model. Climate Dynamics 4,145-156.

[43] Nakamura, M., Stone, P.H., and Marotzke, J., 1994: Destabilization of the thermohaline circulation by atmospheric eddy transports. J. Climate 7,1870-1882.

[44] Nese, J.M., and Dutton, J.A., 1993: Quantifying predictability variations in a low-order ocean-atmosphere model: A dynamical system approach. J. Atm. Sci. 6,185-204.

[45] Oseldec, V.I., 1968: A multiplicative ergodic theorem. Lyapunov characteristic numbers for dynamical systems. Trudy Mosk. Math. Obsc. 19, 197.

[46] Palmer, T.N., 1996: Predictability of the atmosphere and oceans: From days to decades. In: Large-scale transport processes in oceans and atmosphere, D.T.A. Anderson and J. Willebrand, eds., NATO ASI Series vol. 44, Springer, pp. 83-155.

[47] Palmer, T.N., and Sun, Z., 1985: A modelling and observational study of the relationship between sea surface temperatures in the northwest Atlantic and the atmospheric general circulation. Q.J.R. Meteor. Soc. 111,691-713.

[48] Prange, M., Lohmann, G., and Gerdes, R., 1997: Sensitivity of the thermohaline circulation for different climates -Investigations with a simple atmosphere-ocean model. Palaeoclimates (in press)

[49] Rahmstorf, S., 1995: Multiple convection patterns and thermohaline flow in an idealized OGCM. J. Climate 8,3028-3039.

[50] Rahmstorf, S., 1996: On the freshwater forcing and transport of the Atlantic thermohaline circulation. Climate Dynamics 12,799-811.

[51] Rahmstorf, S. and Willebrand, J., 1995: The role of the temperature feedback in stabilizing the thermohaline circulation. J. Phys. Oceanogr. 25,787-805.

[52] Reddy, S.C., 1993: Pseudospectra of Wiener-Hopf integral operators and constant-coefficient differential operators. J. Integral Eqs. Appl. 5,369-403.

[53] Reverdin, G., Cayan, D., Dooley, H.D., Ellet, D.J., Levitus, S., Penhoat, Y., and Dessier, A., 1994: Surface salinity of the North Atlantic: Can we reconstruct its fluctuations over the last hundred years ? Prog. Oceanog. 33,303-346.

[54] Ruddick, B., and Zhang, L., 1996: Qualitative behaviour and nonoscillation of Stommel's thermohaline box model. J. Climate 9,2768-2777.

[55] Sarnthein, M., Winn, K., Jung, S.J.A., Duplessy, J.-C., Labeyrie, L., Erlenkeuser, H., and Ganssen, G., 1994: Changes in east Atlantic deep water circulation over the last 30,000 years: Eight time slice reconstructions. Paleoceanogr. 9,209-267.

[56] Schiller, A., Mikolajewicz, U., and Voss, R., 1996: The stability of the thermohaline circulation in a coupled ocean-atmosphere general circulation model. Climate Dynamics (in press).

[57] Schneider, J., and Lohmann, G., 1997: Exact solution of Jacobi type evolution equations. SIAM Appl. Math. (submitted)

[58] Sellers, W. D., 1969: A global climate model based on the energy balance of the earth-atmosphere system. J. Appl. Meteorol. 8, 392-400.

[59] Stocker, T.F., 1996: An overview of century time-scale variability in the climate system: Observations and models. In: Large-scale transport processes in oceans and atmosphere, D.T.A. Anderson and J. Willebrand, eds., NATO ASI Series vol. 44, Springer, pp. 83-155.

[60] Stommel, H.M., 1961: Thermohaline convection with two stable regimes of flow. Tellus 13,224-230.

[61] Timmermann, A., Latif, M., Voss, R., and Grötzner, A., 1997: North Atlantic interdecadal variability: A coupled air-sea mode. J. Climate (submitted).

[62] Trefethen, L.N., Trefethen, A.E., Reddy, S.C., and Driscoll, T.A., 1993: Hydrodynamic stability without eigenvalues. Science 261,578-584.

[63] Tzipermann, E., 1997: Inherently unstable climate behaviour due to weak thermohaline circulation. Nature 386,592-595.

[64] Van der Schrier, G., and Maas, L.R.M., 1997: Chaos in a simple model of the three-dimensional, salt-dominated ocean circulation. Climate Dynamics (submitted).

[65] Weber, S.L., 1997: Parameter sensitivity of a coupled atmosphere-ocean model. Climate Dynamics (submitted).

[66] Weisse, R., Mikolajewicz, U., and Maier-Reimer, E., 1994: Decadal variability of the North Atlantic in an ocean general circulation model. J. Geophys. Res.89,12411-12421.

[67] Wijffels, S.E., Schmitt, R.W., Bryden, H.L., and Stigebrandt, A., 1992: Transport of fresh water by the oceans. J. Phys. Oceanogr. 22,155-162.

[68] Winton, M., 1997: The effect of cold climate upon North Atlantic Deep Water formation in a simple ocean-atmosphere model. J. Climate 10, 37-51.

[69] Zaucker, F. and Broecker, W.S. 1992: The influence of atmospheric moisture transport on fresh water balance of the Atlantic drainage basin: General circulation model simulations and observations. J. Geophys. Res. 97,2765-2773.

[70] Zhang, S., Greatbatch, R.J., and Lin, C.A., 1993: A reexamination of the polar halocline catastrophe and implications for coupled ocean-atmosphere modeling. J. Phys. Oceanogr. 23,287-299.